理學碩士 學位論文

Synthesis and Photophysical Properties of o-Donor-Acceptor TADF Compounds Containing Oxaborin Acceptor

(옥사보린 받개를 함유하는 오르토-주개-받개
지연형광 화합물의 합성과 광물리적 특성 연구)

蔚 山 大 學 校 大 學 院

化 學 科

金 珠 姬

Synthesis and Photophysical Properties of
o-Donor-Acceptor TADF Compounds
Containing
Oxaborin Acceptor
(옥사보린 받개를 함유하는 오르토-주개-받개
지연형광 화합물의 합성과 광물리적 특성 연구)

指 導 敎 授 이 민 형

이 論文을 理學碩士 學位 論文으로 제출함

2019年 11月

蔚 山 大 學 校 大 學 院

化 學 科

金 珠 姬

金珠姬의 理學碩士 學位 論文을 認准함.

審查委員 정 재 훈   印

審查委員 이 민 형   印

審查委員 홍 종 욱   印

蔚 山 大 學 校 大 學 院

2019년 11月

Synthesis and Photophysical Properties of *o*-Donor-Acceptor TADF Compounds Containing Oxaborin Acceptor

Abstract

Red, green and blue Thermally Activated Delayed Fluorescent (TADF) emitters are being developed for the manufacture of full-color organic light emitting diode (OLED) displays. Although the high efficiency TADF emitters have a theoretical internal quantum efficiency of 100%, there are still problems such as lack of color purity and stability applicable to organic light emitting devices. In this study, 10-Bromo-9-oxa-10-boraanthracene was introduced as an electron acceptor at the 2-position of phenyl ring to develop a highly efficient TADF emitter. As a result, we identified high efficiency TADF properties in the compound introduced with dimethylaridine and phenoxazine as the donor except for *tert*-butyl carbazole. In particular, 100% internal quantum efficiency was observed in the DMAC*o*OB compound in which dimethylacridine was introduced into the electron donor. X-ray single crystal structure analysis of DMAC*o*OB compound showed 90.0 ° dihedral angle of dimethylacridine and oxaborin to phenyl ring. The length between N-B is 2.845 Å which implies that there is a direct interaction between nitrogen and boron. The PL spectra showed a blue to orange emission range varied with introduction of electron donors in a toluene solvent. This is due to the HOMO-LUMO energy gap difference according to the stability of the HOMO. The HOMO-LUMO energy gap measured by cyclic voltammetry showed the same tendency. The result from this study, we suggest the prospect as a third generation OLED emitting material containing the newly introduced oxaborin electron acceptor.

국문초록

전색 유기발광다이오드(Organic Light Emitting Diode: OLED) 디스플레이 제작을 위하여 적녹청색(red, green, blue)의 열활성지연형광(Thermally Activated Delayed Fluorescent: TADF) 발광체가 개발되고 있다. 고효율의 열활성지연형광 발광체는 이론적으로 100%의 내부양자효율을 가지고 있지만 유기 발광 소자에 적용 가능한 색 순도와 안정성 결여 등과 같은 문제가 있어 아직 많은 연구가 필요하다. 본 연구에서는 고효율의 열활성지연형광 발광체를 개발하기 위해 페닐고리 2-위치에 10-Bromo-9-oxa-10-boraanthracene 을 전자 받개로 도입하였다. 그 결과 부틸카바졸을 제외한 다이메틸아크리딘과 페녹사진을 전자주개로 도입한 화합물에서 고효율의 열활성지연형광 특성을 규명하였다. 특히 다이메틸아크리딘을 전자 주개로 도입한 DMACαOB 화합물 에서 100%의 내부양자효율이 관찰되었다. DMACαOB 화합물에 대한 X-선 단결정 구조분석 연구를 통해 페닐고리에 대한 다이메틸아크리딘과 옥사보린의 이면각이 90.0° 으로 관찰되었다. N-B 간의 길이는 2.845 Å으로 이는 질소와 보론 사이에서 직접적인 인력이 존재함을 암시한다. 광물리적 특성을 조사한 결과 Toluene 용매에서 전자 주개 도입의 따라 청색에서 주황색의 발광 범위를 나타냈다. 이는 HOMO의 안정도에 따른 HOMO-LUMO 에너지 갭 차이에서 기인된다. 순환전압전류법을 통한 HOMO-LUMO 에너지 갭을 측정한 결과 같은 경향성을 가지는 것을 확인하였다. 본 연구의 결과는 새롭게 도입한 옥사보린 전자 받개를 함유한 3세대 OLED 발광재료로서의 전망을 제시한다.

Contents

List of Figures

List of Schemes

List of Tables

I. Introduction

1-1. Organic light-emitting diodes (OLEDs)

Organic light emitting diodes (OLEDs) is a display that emits by combining holes injected from the electrons and electrons injected from the cathode using organic thin film layer which form a p-n junction. OLEDs are characterized by low driving voltage, high brightness, full-color emission, rapid response, and easy fabrication of potentially large area, flexible thin-film devices.[1] Since the first discovery of luminescence in anthracene single crystal by W.Helfirich, *et al*. in 1965, research and development for full-fledged commercialization have started with reporting a double-layered device using tris(8-hydroxyquinoline) aluminum (Alq_3) as the emitting and electron-transporting layer by Tang and VanSlyke at Eastman Kodak in 1987.[1, 2] The driving-voltage was lowered below 10 V and the efficiency was improved up to 1.5l m/W. By using the doping method, electroluminescence (EL) performance has increased by 2-3 fold. The researches on electroluminescence were boosted by the pioneering effort of Tang and VanSlyke and the resulting a great deal of activity in lots of research groups.[3] The first OLEDs as flat displays that used the form of organic polymers light emitting were commercialized in 1997. Nowadays, OLED displays have speedily expanded their market. The reason for remarkable attention in OLEDs is due to technological aspects such as, affordable costs, the simplicity of fabrication using vacuum deposition or solution processing.[4] have a number of advantages such as, the possibility of realizing light weight and flexible plastic substrates or large-area displays, better power efficiency and thickness. Though OLEDs already satisfy the requirements for some realistic applications in, e.g., portable electronics like laptop computers and digital cameras, smart phones with operating lifetimes about 100,000 hours, the intrinsic limitations of OLEDs have not yet been reached. So more scientific efforts committed to the design, engineering and production of OLEDs considering interfaces, charge carrier injection, quenching processes, spin effects, morphology changes or light extraction should be made up for providing a step ahead to the full commercialization of this technology.[3, 4]

1-2. Multi-layer OLEDs

The general structure of an OLED is a structure in which a transparent indium tin oxide (ITO) anode layer is formed on a transparent substrate such as glass, and a multilayer thin film of various organic materials having different transport capacities and a cathode of an Mg-Ag alloy are sequentially formed. The multi-layered thin film has a hole injection layer (HIL) containing a metal complex salt of C_0 and G_a from the anode side, a hole transport layer (HTL), and an emitting layer (EML) which is composed of an electron transport layer (ETL) such as Al-poly (*p*-phenylene vinylene), and this organic thin film is about 100 nm. In the hole transport layer, electron donor molecules having small ionization potential are used to facilitate hole injection from the anode.[5] The emission layer which emits red, blue, and green light by recombination of injected electrons and holes, and its spectrum is determined according to the binding energy in the emission layer.[3, 6] Therefore, the emission color is determined depending on the emission layer forming material. The electron transport layer easily transports electrons supplied from the cathode to the light emitting layer and suppresses movement of holes that are not bonded in the light emitting layer. In addition, the electron affinity should be excellent since it increases the recombination opportunity in the light emitting layer.[1, 2, 6] By lowering the difference of the energy barriers, Hole-injecting layer helps the hole injecting from anode to hole-transporting layer. Hole-transporting materials assist in accepting holes from hole-injecting layer and transporting them to emitting layer. Electron injecting layer sandwiched between the cathode and the electron-transporting layer helps in lowering the difference of the energy barriers from the cathode into the electron-transporting layer. Electron-transporting materials assist receiving electrons from the electron-injection layer and deliver electrons to emitting layer. The holes and electrons transported through the hole-transporting layer and electron-transporting layer are recombined to generate excitons in the emitting layer. Light emission proceeds via a recombination of electrons and holes.[3, 5, 6]
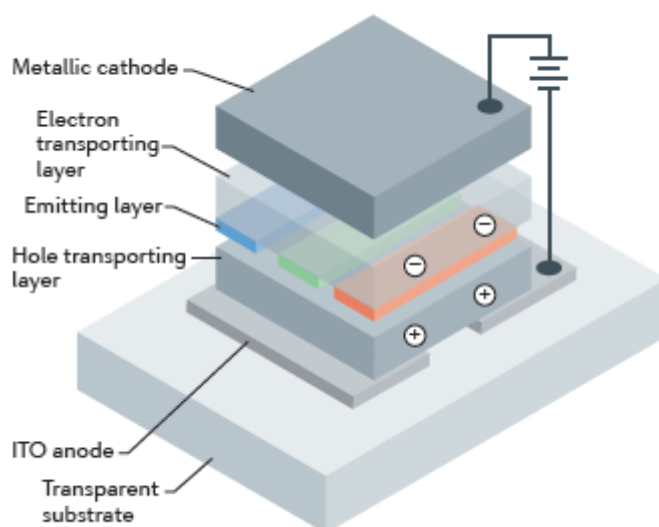
Figure 1. Schematic overview of OLED device.

1-3. Working Principle of OLEDs

When voltage is applied between the two electrodes, holes are injected from the anode and electrons are injected from the cathode, and they reach the light emitting layer along the electron transport layers, respectively, where electrons and holes meet to form an exciton. The light emitting layer gets light by recombination of exciton and becomes a ground state.[7] The emission wavelength is determined by the energy difference of the exciton which is the energy difference between HOMO and LUMO, and generates light emitting toward the transparent electrode. When the electrons and holes having spin $S = 1/2$ form excitons in the light emitting layer, the triplet which is $S = 1$ where the two spins are arranged in symmetry and the singlet which is $S = 0$ where the two spins are arranged in asymmetry are generated in a 3:1 ratio.[8] General organic materials do not emit light in the triplet state.[6] By quantum mechanical selectivity, singlet excitons emit and transit to the ground state. This is called fluorescence. Therefore, the internal quantum efficiency of the theoretical OLED device is up to 25%. Triplet exciton generation can be formed by intersystem crossing (ISC) from singlet excitons, or by cleavage of two triplet excitons in a higher excited singlet exciton state.[1, 9, 10]
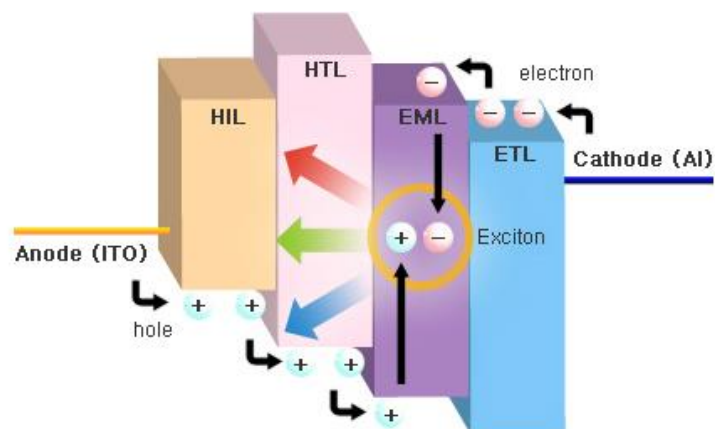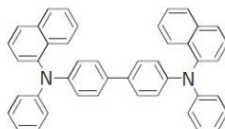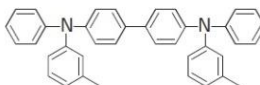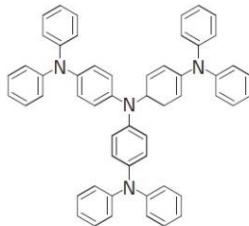
.

Figure 2. Working principle of OLEDs
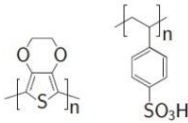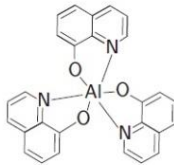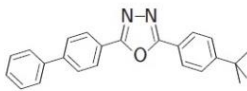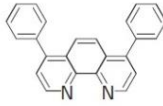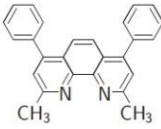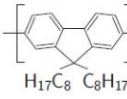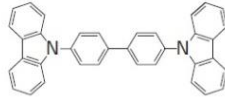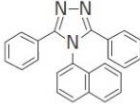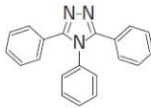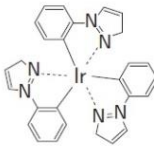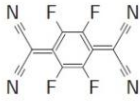
Figure 3. Structures of OLED materials used for each layer.

1-4. Thermally Activated Delayed Fluorescence (TADF)

The 1st generation of oleds is limited by their poorly 25% internal quantum efficiency (IQE) since only a quarter of singlet excitons can be generated. The 2nd generation of oleds can overcome this limitation by introducing heavy metal elements (Ir and Pt) which can be permitted spin-orbit coupling (SOC).[11,12] However, phosphorescence emitters still have some problem such as high cost, toxicity, and instability of materials containing heavy metals. To achieve highly efficient emitters using triplet excited state without expensive heavy metals, thermally activated delayed fluorescence (TADF) has been discovered by Adachi *et al.* in 2011.[13, 14] Since that discovered, TADF materials have been actively researched as efficient emitters of 3rd generation of OLEDs. Because TADF materials have theoretically 100% IQE from reverse intersystem crossing (RISC) of excited triplet state without nonradiative decay.[9, 15]
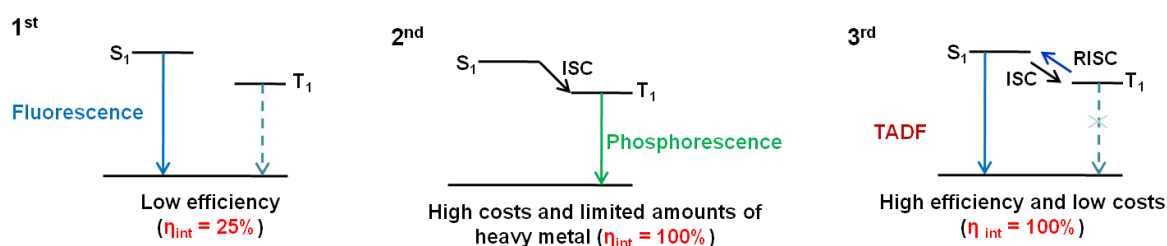
Figure 4. The Generation of OLEDs.

In a TADF process, a small energy gap (ΔE_{ST}) between singlet excited state and triplet excited state is most important factor for achieving efficient spin up-conversion from triplet to singlet states. It is generally known that $\Delta E_{ST} < 0.2$ eV is favorable for an efficient RISC process.[4, 16] Enhanced RISC followed by delayed fluorescence (S_1 to S_0) with longer lifetime than the prompt fluorescence. The most typical method for obtaining small energy splitting between the excited states in organic molecule is twisted donor structure allowing for effective reduction in the spatial overlap between the highest occupied molecular orbitals (HOMO) and the lowest unoccupied molecular orbitals (LUMO).[11, 15, 17]
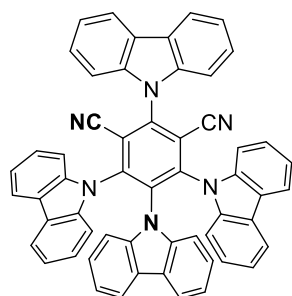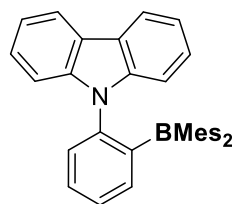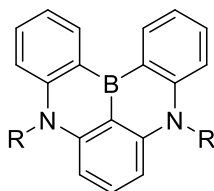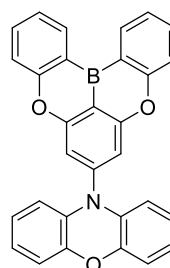
Figure 5. Structures of TADF emitters.

Therefore molecular rigidity is important to achieve TADF efficiently. Different conformations of a molecule can yield different TADF efficiencies, consequently flexible donors or acceptors should be avoided.[15,18] *ortho* D−A connectivity, as the donor and acceptor groups in the *ortho* position make higher steric hindrance due to the close proximity. Moreover, combining the *ortho* D−A structure with a bulky donor or acceptor could synergistically reinforce the potential benefit of inherent steric "locking" between donor and acceptor groups.[19,21] And also it could be achieved by a large dihedral angle (θ) in a twisted donor–acceptor bipolar structure caused by bulky substituents or a spiro-junction.[21]

2. TADF emitters containing triarylboron

The triarylboron is named as the compounds which connect one boron atom and three benzene derivatives. The vacant p orbital on the three-coordinate boron center raise electron accepting ability.[15] High Lewis acidic triarylboron compound in D-A organic π-conjugated system function as good acceptor through p_π-π* conjugation.[16, 20] When accompanied by appropriate electron donors such as amines, these molecules possess large electronic dipoles, which promote donor-acceptor strong intramolecular charge-transfer (ICT) upon excitation with light.[22] Triarylboron based D-A compounds strongly influence their photophysical properties, and makes them useful for non-linear optics, anion sensing, hydrogen activation and storage, optoelectronics, and TADF emitters.[4, 13, 23] However, limited a number of triarylboron D-A compounds have been used as emitters in organic light-emitting diodes (OLEDs) because the external quantum efficiency of such devices has been relatively low.[24]
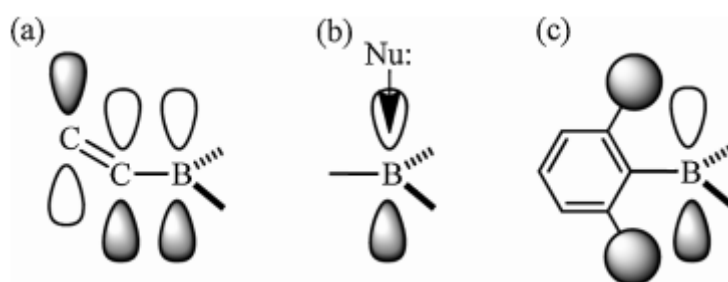
Figure 6. Characteristic features of boron atom in the π-conjugated materials.

3. Research Scopes

Thermally activated delayed fluorescence materials have attracted attention because TADF emitters can theoretically harvest 100% of excitons through the reverse intersystem crossing (RISC).[19] To achieve efficient TADF character, *Ortho* donor-acceptor compounds where oxaboraanthracene as acceptor with various electron-donating group as donors, such as *tert*-butylcarbazole (**BuCzoOB**), dimethylacridine (**DMACoOB**), as well as phenoxazine (**PXZoOB**) were synthesized in several steps. For comparison, dimesitylboron acceptor containing compound was also prepared (**DMACoB**). All compounds were analyzed by NMR spectroscopy. **DMACoOB** and **DMACoB** structures were analyzed by single crystals suitable for X-ray crystallography obtained by slow evaporation of a solution. In addition, UV-Vis absorption and emission spectra as well as emission lifetimes were measured in toluene solution to study the photophysical properties. In this study, we found the direct interaction between nitrogen-boron atoms in X-ray data of **DMACoOB** compared with **DMACoB**. And also we investigated the effects of different donors on the TADF molecules of *ortho* donor-acceptor compounds.

II. Experimental

1. **Chemical and instrumentation**

All operations were performed under an inert nitrogen atmosphere using standard Schlenk and glovebox techniques. Anhydrous grade solvents (Aldrich) were dried by passing them through an activated alumina column and stored over activated molecular sieves (5 Å). Spectrophotometric-grade solvents for photophysical measurements were used as received from Aldrich and Merck. Commercial reagents were used without further purification after purchase. Deuterated solvents from Cambridge isotope Laboratories were used. NMR spectra were recorded on a Bruker AM 300 (300.13 MHz for ^{1}H, 75.48 MHz for ^{13}C, 96.29 MHz for ^{11}B) spectrometer at ambient temperature. Chemical shifts are given in parts per million (ppm), and are referenced against external Me$_4$Si (^{1}H, ^{13}C), BF$_3$OEt$_2$ (δ 0 ppm, ^{11}B). Elemental analyses were performed on a Flash 2000 elemental analyzer (Thermo Scientific) at University of Ulsan. Melting point (mp) was measured by Melting Point Apparatus SMP30 (Stuart Equipment). Thermogravimetric analysis (TGA) was performed with a TA Instruments Q50 under an N$_2$ atmosphere at a heating rate of 10 ℃/min. Mass spectra were obtained on a JEOL JMS700 high-resolution EI-mass spectrometer (HR EI-MS) at the Korea Basic Science Institute, Daegu, Korea. Cyclic voltammetry experiments were performed using an Autolab/PGSTAT101 system.

2. Synthesis

All compounds were prepared according to **Scheme 1.** 3,6-Di-*tert*-butyl-9-(2-bromo-3-methylphenyl)-9*H*-carbazole (**BuCz*o*Br**), 1-iodo-2-bromo-3-methylbenzene, and 10-bromo-9-oxa-10-boraanthracene were prepared from the reported procedure.[4, 25, 26] Full experimental details are given below.

3,6-Di-*tert*-butyl-9-(2-bromo-3-methylphenyl)-9*H*-carbazole (BuCz*o*Br, 1a)
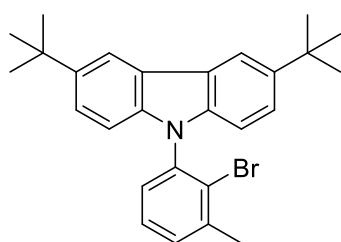
A suspension of 2-bromo-1-fluoro-3-methylbenzene (1.5 g, 7.94 mmol), 3,6-di-*tert*-butyl-9*H*-carbazole (2.22g, 7.94 mmol) and Cs_2CO_3 (5.17 g, 15.9 mmol) in 15 mL dry DMF was stirred and heated to 150 °C for 12 h under nitrogen atmosphere. The reaction mixture was poured into 200 mL of water and the precipitate formed was collected by filtration. The crude product was purified by column chromatography using CH_2Cl_2/*n*-hexane (1:10, v/v) as an eluent to give **1a** as a white powder (Yield: 2.31 g, 65%). ^{1}H NMR (300 MHz, CDCl₃) δ 8.19 (d, *J* = 1.7 Hz, 4H), 7.52 – 7.37 (m, 1H), 7.29 (dd, *J* = 6.9, 2.3 Hz, 2H), 7.01 (d, *J* = 8.6 Hz, 3H), 2.60 (s, 2H), 1.50 (s, 18H).

10-(2-Bromo-3-methylphenyl)-9,9-dimethyl-9,10-dihydroacridine (DMAC*o*Br, 2a)
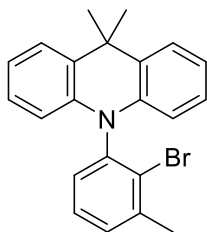
A solution of $Pd_2(dba)_3$ (0.22 g, 0.24 mmol), tri-*tert*-butylphosphine (0.09 g, 0.43 mmol), NaO*t*Bu (0.92 g, 9.56 mmol), 1-iodo-2-bromo-3-methylbenzene (1.70 g, 5.73 mmol) and 9,9-dimethyl-9,10dihydroacridine (1.00 g, 4.78 mmol) in toluene (50 ml) was stirred at 80 °C for 24 h. After cooling down to room temperature, water (100 mL) was slowly added and a turbid mixture was extracted with CH_2Cl_2 (50 mL × 3). The organic layer was dried over MgSO₄, filtered, and concentrated under reduced pressure. The crude product was purified by silica gel column chromatography using CH_2Cl_2/*n*-hexane (1:5, v/v) as an eluent to give **2a** as a white powder (yield: 1.03 g, 57%). ^{1}H NMR (300 MHz, CD₂Cl₂) δ 7.59 – 7.39 (m, 4H), 7.25 (dd, *J* = 7.2, 2.1 Hz, 1H), 7.08 – 6.85 (m, 4H), 6.23 – 6.00 (m, 2H), 2.59 (s, 3H), 1.75 (d, *J* = 23.1 Hz, 6H). ^{13}C NMR (CD₂Cl₂) δ 141.7, 139.7, 139.2, 130.7, 130.4, 129.8, 129.1, 128.6, 126.5, 125.8, 120.7, 113.3, 35.9, 33.3, 31.3, 23.6. HRMS (EI): *m/z* calcd for $C_{22}H_{20}BrN$, 379.0779; found, 379.0777.

10-(2-Bromo-3-methylphenyl)-10*H*-phenoxazine (PXZ*o*Br, 3a)
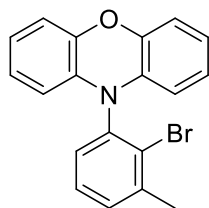
This compound was prepared in a manner analogous to the synthesis of **2a** using 2-Bromo-1-iodo-3-methylbenzene (1.21 g, 4.08 mmol), Pd$_2$(dba)$_3$ (150 mg, 0.16 mmol), tri-*tert*-butylphosphine (50 mg, 0.25 mmol), 10*H*-phenoxazine (0.5 g, 2.73 mmol) and NaO^{t}Bu (0.66 g, 6.86 mmol) to give **3a** as a white powder (Yield: 0.616 g, 64%). ^{1}H NMR (300 MHz, CD$_2$Cl$_2$) δ 7.50 – 7.34 (m, 2H), 7.33 – 7.20 (m, 1H), 6.75 – 6.52 (m, 6H), 5.85 – 5.72 (m, 2H), 2.52 (s, 3H). ^{13}C NMR (CD$_2$Cl$_2$) δ 144.1, 142.2, 137.6, 133.2, 131.5, 130.5, 129.7, 128.6, 123.7, 123.7, 121.8, 121.8, 115.7, 113.2, 23.9. HRMS (EI): *m/z* calcd for C$_{19}$H$_{14}$BrNO, 351.0259; found, 351.0257.

1,1'-oxybis[2-(trimethylsilyl)]-benzene (1b)
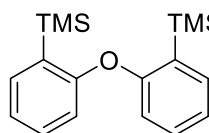
To a solution of diphenyl ether (0.9 mL, 5.68 mmol) in dry ether (20 mL) was added dropwise *n*-BuLi (5.0 mL, 12.5 mmol) at −78 °C under nitrogen and heated to 60 ℃ for 72 h. After cooling to −78 °C, chlorotrimethyl silane (1.59 mL, 12.5 mmol) was slowly added and stirred at 60 ℃ for 12 h. The resulting solution was quenched by the addition of a saturated aqueous NH$_4$Cl solution (50 mL), extract with diethyl ether (30 mL × 3). The combined organic layer was dried over MgSO$_4$, filtered and concentrated under reduced pressure. The crude oil was purified by silica gel column chromatography using only *n*-Hexane as an eluent to give **1b** as a colorless oil. ^{1}H NMR (300 MHz, CDCl$_3$) δ 7.49 (dd, *J* = 7.3, 1.8 Hz, 2H), 7.26 (ddd, *J* = 8.3, 4.9, 1.8 Hz, 2H), 7.08 (td, *J* = 7.3, 0.8 Hz, 2H), 6.64 (d, *J* = 8.1 Hz, 2H), 0.31 (s, 18H).

10-Bromo-9-oxa-10-boraanthracene (2b)
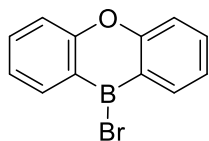
A solution of boron tribromide (1.95 mL, 20.2 mmol) in dry CH_2Cl_2 (10 mL) was added dropwise under nitrogen to a solution of **1b** (2.12 g, 6.74 mmol) in dry CH_2Cl_2 (10 mL) at -78 °C. This reaction mixture was allowed to warm to room temperature and stirred for 1 h. The solvent and residues were removed by vacuum. The compound was not purified any further method (gray powder, Yield: 2.31 g, 89%). ^{1}H NMR (300 MHz, CDCl$_3$) δ 8.34 (dd, J = 7.7, 1.7 Hz, 2H), 7.81 (ddd, J = 8.7, 7.1, 1.8 Hz, 2H), 7.57 (d, J = 8.2 Hz, 2H), 7.40 (ddd, J = 7.9, 7.1, 1.0 Hz, 2H).

9-(2-(10*H*-Dibenzo[*b,e*][1,4]oxaborinin-10-yl)-3-methylphenyl)-3,6-di-*tert*-butyl-9*H*-carbazole (BuCz*o*OB, 1c)
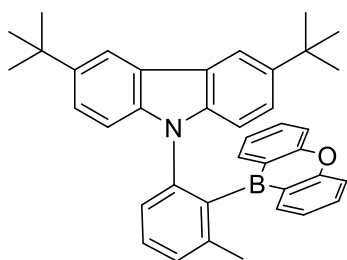
To a solution of **1a** (0.289 g, 0.64 mmol) in dry ether (10 mL) was added dropwise *n*-BuLi (0.28 mL, 0.7 mmol) at −78 °C. The reaction mixture was stirred at −78 °C for 1 h. After that the solution of **2b** (0.2 g, 0.77 mmol) in dry toluene was slowly added. After stirring at room temperature for 12 h, the solution was concentrated under reduced pressure. It was recrystallized in CH_2Cl_2/methanol to give **BuCz*o*OB**, **1c** as a white crystal (Yield: 0.218 g, 62%). ^{1}H NMR (300 MHz, CD$_2$Cl$_2$) δ 7.75 − 7.67 (m, 4H), 7.60 (t, J = 7.7 Hz, 1H), 7.52 (m, 3H), 7.37 (d, J = 7.4 Hz, 1H), 7.28 − 7.21 (m, 2H), 7.00 (m, 6H), 2.26 (s, 3H, –C*H*$_3$), 1.29 (s, 18H, –C(C*H*$_3$)$_3$). ^{13}C NMR (CD$_2$Cl$_2$) δ 159.2, 142.4, 141.9, 140.9, 140.5, 136.5, 134.6, 129.7, 129.3, 126.3, 123.2, 122.9, 121.9, 117.4, 115.7, 111.2 (Ar–*C*), 34.8, 32.0 (–C*H*$_3$). ^{11}B NMR (CD$_2$Cl$_2$): δ 53.6. Anal. Calcd for $C_{39}H_{38}BNO$: C, 85.55; H, 7.00; N, 2.56. Found: C, 85.28; H, 7.01, N, 2.72. mp = 208 °C. T_{d5} = 285 °C.

10-(2-(10*H*-Dibenzo[*b*,*e*][1,4]oxaborinin-10-yl)-3-methylphenyl)-9,9-dimethyl-9,10-dihydroacridine (DMAC*o*OB, 2c)
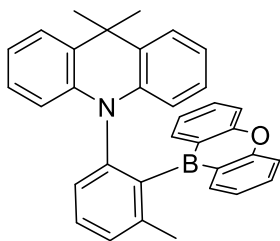
This compound was prepared in a manner analogous to the synthesis of **1c** using **2a** (0.170 g, 0.45 mmol), *n*-BuLi (0.20 mL, 0.49 mmol), **2b** (0.14 g, 0.54 mmol) to give **DMAC*o*OB**, **2c** as a faint green crystal (Yield: 0.107 g, 50%). ^{1}H NMR (300 MHz, CD$_2$Cl$_2$) δ 7.73 – 7.46 (m, 6H), 7.42 – 7.33 (m, 2H), 7.25 (d, *J* = 7.9 Hz, 1H), 7.09 (dd, *J* = 7.7, 1.5 Hz, 2H), 7.00 – 6.87 (m, 4H), 6.75 (td, *J* = 7.5, 1.3 Hz, 2H), 6.61 (dd, *J* = 8.2, 1.2 Hz, 2H), 2.17 (s, 3H), 1.57 (s, 3H), -0.00 (s, 3H). ^{13}C NMR (CD$_2$Cl$_2$) δ 158.9, 143.2, 142.3, 141.3, 136.4, 134.5, 130.2, 129.4, 128.9, 128.6, 125.5, 123.4, 121.5, 120.4, 116.8, 115.0 (Ar–*C*), 35.4, 30.7, 24.4, 22.3 (–*C*H$_3$ and –*C*(*C*H$_3$)$_2$). ^{11}B NMR (CD$_2$Cl$_2$): δ 54.5. Anal. Calcd for C$_{34}$H$_{28}$BNO.CH$_2$Cl$_2$: C, 83.09; H, 5.79; N, 2.83. Found: C, 82.83; H, 5.75; N, 2.98. mp = 208 °C. T_{d5} = 238 °C.

10-(2-(10*H*-Dibenzo[*b*,*e*][1,4]oxaborinin-10-yl)-3-methylphenyl)-10*H*-phenoxazine (PXZ*o*OB, 3c)
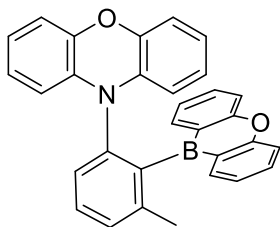
This compound was prepared in a manner analogous to the synthesis of **1c** using **3a** (0.150 g, 0.43 mmol), *n*-BuLi (0.19 mL, 0.47 mmol), **2b** (0.132 g, 0.51 mmol) to give **PXZ*o*OB**, **3c** as a yellow crystal (Yield: 0.087 g, 45%). ^{1}H NMR (300 MHz, CD$_2$Cl$_2$) δ 7.68 – 7.53 (m, 5H), 7.52 – 7.40 (m, 3H), 7.30 (d, *J* = 7.8 Hz, 1H), 6.99 (ddd, *J* = 8.0, 7.0, 1.1 Hz, 2H), 6.46 (dtd, *J* = 23.4, 7.5, 1.6 Hz, 4H), 6.29 (dd, *J* = 7.7, 1.6 Hz, 2H), 6.21 (dd, *J* = 7.8, 1.6 Hz, 2H), 2.16 (s, 3H, –*C*H$_3$). ^{13}C NMR (CD$_2$Cl$_2$) δ 159.5, 143.6, 136.8, 134.9, 130.3, 129.4, 123.1, 122.0, 117.6, 115.3 (Ar–*C*), 22.80 (–*C*H$_3$). ^{11}B NMR (CD$_2$Cl$_2$): δ 54.6. Anal. Calcd for C$_{31}$H$_{22}$BNO$_2$: C, 82.50; H, 4.91; N, 3.10. Found: C, 82.36; H, 4.72; N, 3.30. mp = 245 °C. T_{d5} = 277 °C.

10-(2-(Dimesitylboranyl)-3-methylphenyl)-9,9-dimethyl-9,10-dihydroacridine (DMAC*o*B, 4c)
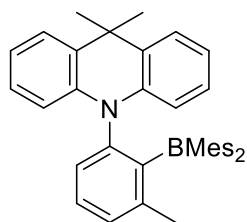
To a solution of **2a** (0.30 g, 0.79 mmol) in dry ether (20 mL) was added dropwise *n*-BuLi (0.35 mL, 0.87 mmol) at −30 °C. The reaction mixture was stirred at −30 °C for 1 h and then the solution of dimesitylboron fluoride (0.26 g, 0.95 mmol) in dry ether was slowly added. After stirring at room temperature for 12 h, the resulting green solution was quenched by the addition of a saturated aqueous NH_4Cl solution (50 mL), extract with diethyl ether (30 mL), and washed with water (50 mL × 3). The combined organic layer was dried over $MgSO_4$, filtered and concentrated under reduced pressure. The crude product was purified by silica gel column chromatography using CH_2Cl_2/*n*-Hexane (1:8 v/v) as an eluent to give **DMAC*o*B**, **4c** as a green crystal (Yield: 0.217 g, 50%). ^{1}H NMR (300 MHz, CD_2Cl_2) δ 7.53 (t, J = 7.7 Hz, 1H), 7.32 (ddd, J = 6.9, 5.2, 1.2 Hz, 2H), 7.11 − 7.00 (m, 2H), 6.85 (m, 2H), 6.76 − 6.62 (m, 4H), 6.36 (dd, J = 8.0, 1.4 Hz, 1H), 6.31 (s, 1H), 6.14 (s, 1H), 5.95 − 5.86 (m, 1H), 2.23 (s, 3H), 2.16 (d, J = 8.3 Hz, 6H), 2.07 (s, 3H), 1.90 (d, J = 27.5 Hz, 6H), 1.60 (s, 3H), 1.41 (s, 6H). ^{13}C NMR (CD_2Cl_2) δ 147.1, 145.2, 142.5, 142.0, 141.9, 141.8, 140.4, 139.0, 137.9, 137.5, 132.8, 131.7, 131.0, 130.6, 130.0, 129.7, 128.7, 128.6, 128.1, 126.8, 125.8, 125.5, 125.1, 120.3, 119.9, 117.5, 116.2 (Ar–*C*), 35.9, 34.9, 34.7, 26.0, 24.2, 23.2, 23.7, 22.7, 21.2, 21.0 (–*C*H$_3$). ^{11}B NMR (CD_2Cl_2): δ 80.5. Anal. Calcd for $C_{40}H_{42}BN$: C, 87.74; H, 7.73; N, 2.56. Found: C, 87.24; H, 7.74; N, 2.70. mp = 223 °C. T_{d5} = 285 °C.

3. X-ray crystallography

A specimen of suitable size and quality was coated with Paratone oil and mounted onto a glass capillary. The crystallographic measurement was performed using a Bruker Apex II-CCD area detector diffractometer, with graphite-monochromated MoKα radiation (λ = 0.71073 Å). The structure was solved by direct methods, and all nonhydrogen atoms were subjected to anisotropic refinement by full-matrix least-squares on F^2 by using the SHELXTL/PC package. Hydrogen atoms were placed at their geometrically calculated positions and were refined riding on the corresponding carbon atoms with isotropic thermal parameters.

4. Photophysical measurements.

UV-Vis absorption and PL spectra were recorded on a Varian Cary 100, a HORIBA FluoroMax-4P spectrophotometer and a FS5 spectrophotometer, respectively. Solution PL spectra were obtained from oxygen-free and air-saturated toluene solutions (typically 50 μM in toluene). Absolute photoluminescence quantum yields (PLQYs, Φ_{PL}) of solutions were measured on an absolute PL quantum yield spectrophotometer (Quantaurus-QY C11347-11, Hamamatsu Photonics) equipped with a 3.3 inch integrating sphere. Transient PL decays were measured on an FS5 spectrophotometer (Edinburgh Instruments) in either time-correlated single-photon counting (TCSPC) mode (an EPL-375 ps pulsed diode laser as a light source) or multi-channel scaling (MCS) mode (a microsecond Xenon flashlamp as a light source). The lifetimes of prompt fluorescence (τ_p) were estimated by fitting decay curves measured via the TCSPC mode, while those of delayed fluorescence (τ_d) were estimated with curves measured via the MCS mode. The temperature-dependence of PL decay was obtained with an OptistatDN^{TM} cryostat (Oxford Instruments).

5. Cyclic voltammetry

Cyclic voltammetry measurements were carried out in CH_3CN (1×10^{-3} M) with a three-electrode cell configuration consisting of platinum working and counter electrodes and a Ag/AgNO$_3$ (0.01 M in CH_3CN) reference electrode at room temperature. Tetra-n-butylammonium hexafluorophosphate (0.1 M in CH_3CN) was used as the supporting electrolyte. The redox potentials were recorded at a scan rate of 100 mV/s and are reported with reference to the ferrocene/ferrocenium (Fc/Fc$^+$) redox couple.

III. Results and Discussion

1. Synthesis and characterization.

A series of *ortho*-donor-appended compounds with different donors (**BuCz*o*OB, DMAC*o*OB and PXZ*o*OB**) were prepared according to **Scheme 1**. For comparison, dimesitylboron acceptor containing compound was also prepared (**DMAC*o*B**). The phenylene-linker group, 2-bromo-1-iodo-3-methylbenzene, was prepared from 2-bromo-3-methylaniline via Sandmeyer reaction. The **DMAC*o*Br** and **PXZ*o*Br** were prepared using Buchwald-Hartwig amination.[4, 25] **BuCz*o*Br** was prepared using cesium carbonate via cesium salt. And 9-o also 10-bromo-oxa-10-boraanthracene acceptor was prepared from the reported procedure.[26, 27] The final *ortho*-donor-appended compounds containing oxaborin and dimesitylboron acceptors were obtained via lithium salt derived from the *ortho*-donor substituted 2-boromo-3-methylbenzene, followed by reaction with 10-bromo-9-oxa-10-boraanthracene and dimesitylboron fluoride.[19] The methyl group in *meta* position was introduced adjacent to the boron moiety to prevent nucleophilic attack to the boron center and strengthen the rigidity of molecule. All final compounds were characterized by multinuclear NMR spectroscopy (**Figure 7-12**) and elemental analysis.
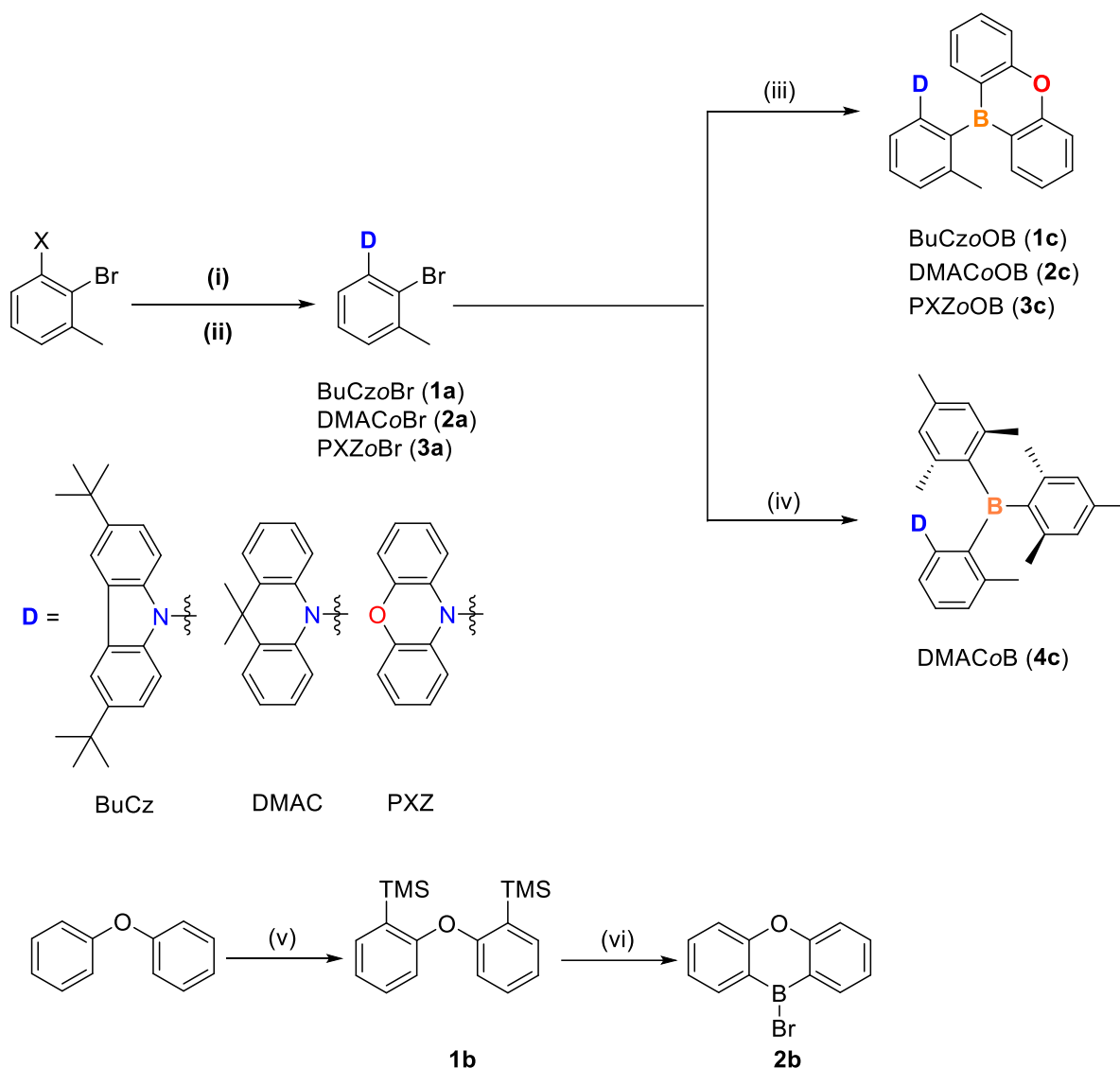
Scheme 1. Condition : (i) X= I, 10*H*-phenoxazine (**3a**), 9,9-dimethyl-9,10-dihydroacridine (**2a**), Pd$_2$(dba)$_3$, P(*t*-Bu)$_3$, Na^{t}OBu, toluene, 60 °C; (ii) X= F, 3,6-di-*tert*-butyl-9*H*-carbazole, Cs$_2$CO$_3$, DMF, reflux (**1a**); (iii) *n*-BuLi, Et$_2$O, −78 °C, then 10-bromo-9-oxa-10-boraanthracene, toluene; (iv) *n*-BuLi, Et$_2$O, −78 °C, then Mes$_2$BF; (v) *n*-BuLi, Et$_2$O, −78 °C, reflux, 72 h, then TMSCl, reflux, 12 h; (vi) BBr$_3$, CH$_2$Cl$_2$, −78 °C.

The ^{1}H NMR spectra of all compounds exhibits singlet of CH$_3$ group (δ 2.16 – 2.26 ppm) substituted at the same phenyl backbone. The ^{1}H NMR spectra of the **DMAC*o*OB** showed two sharp singlet of (CH$_3$)$_2$ from dimethylacridine (δ 1.57 and 0.00 ppm). And also **DMAC*o*B** showed several sharp CH$_3$ peaks from BMes$_2$ group. As for ^{11}B NMR, a tri-coordinated boron center was detected as a broad singlet at δ +80.5 ppm for **DMAC*o*B,**

which is consistent with the presence of trigonal planar boron center from BMes$_2$ group. In contrast with **BuCzoOB**, **DMACoOB** and **PXZoOB** which have cyclic and planarized structure, shifting to the upfield region (ca. δ +53.6, 54.5, 54.7 ppm) was observed. Furthermore, from TGA analysis shows thermal stability, giving T$_{d5}$ value of 285 ^{o}C, 270 ^{o}C, 277 ^{o}C and 285 for **BuCzoOB**, **DMACoOB**, **PXZoOB** and **DMACoB** respectively.

a)
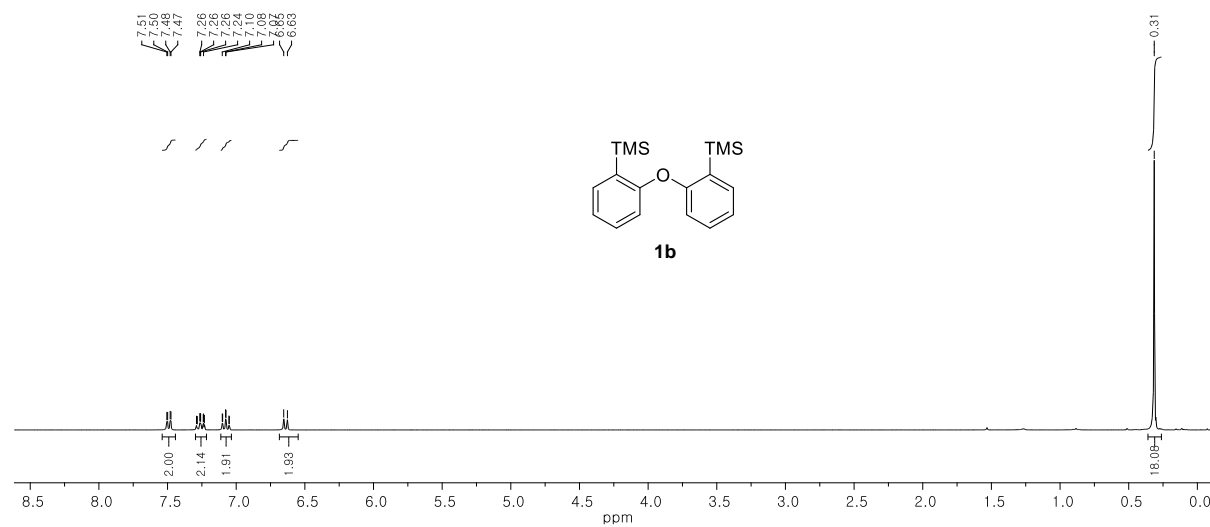
b)
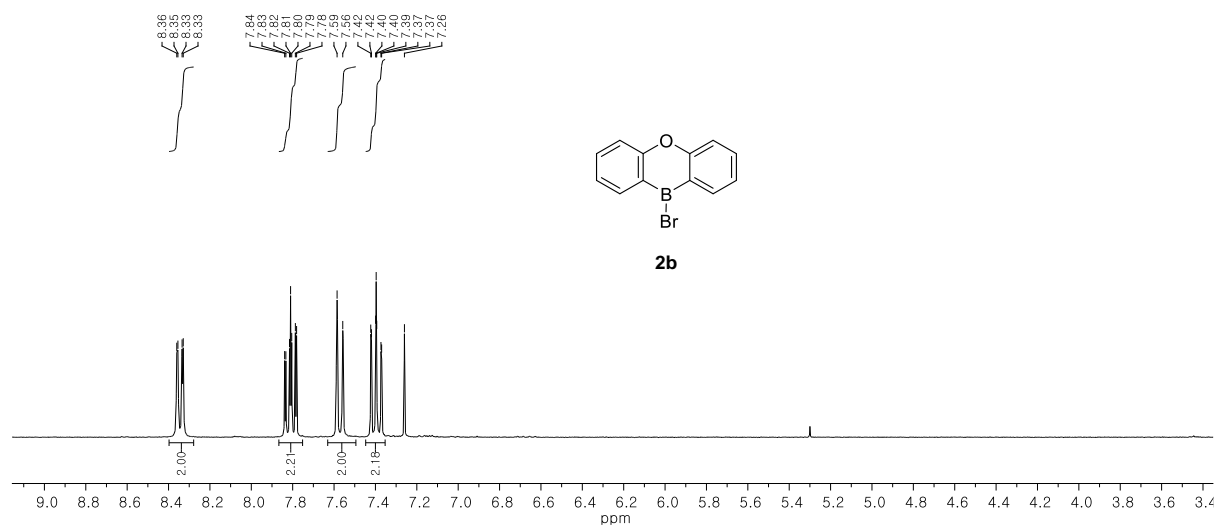
Figure 7. ^{1}H NMR spectra of (a) **1b** and (b) **2b** in CDCl$_3$.

a)

BuCzoBr (**1a**)

b)

DMACoBr (**2a**)

c)
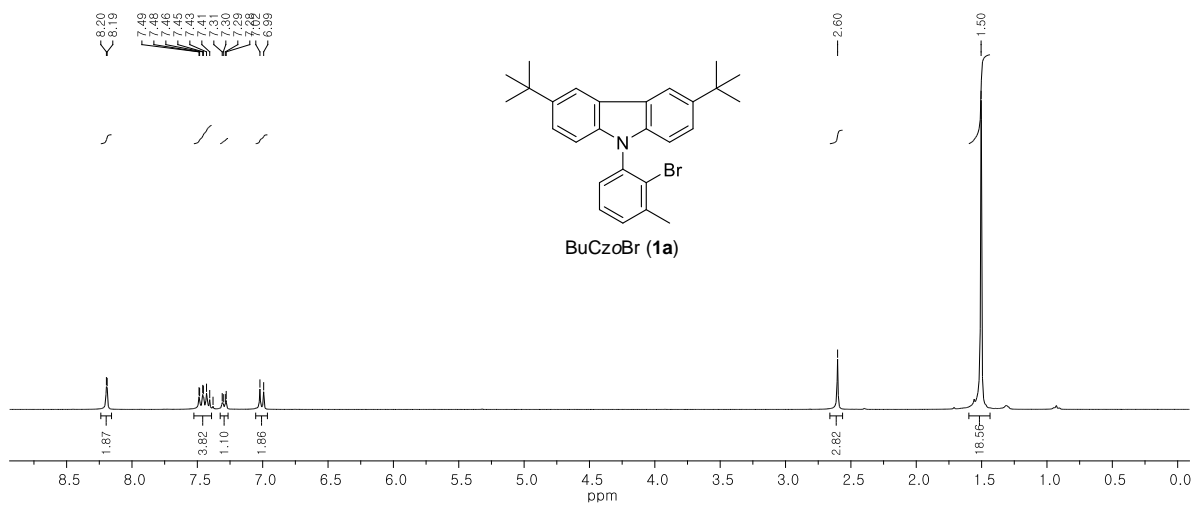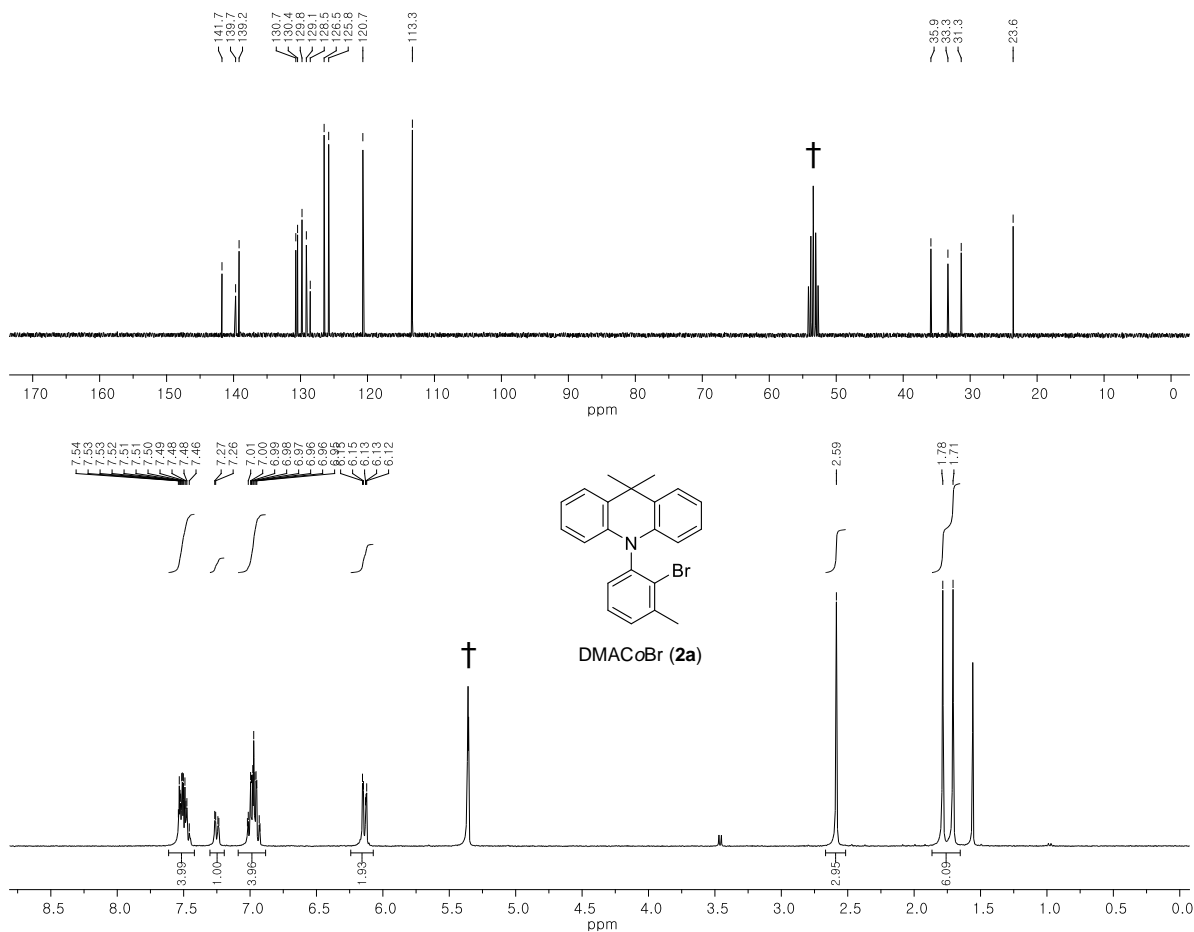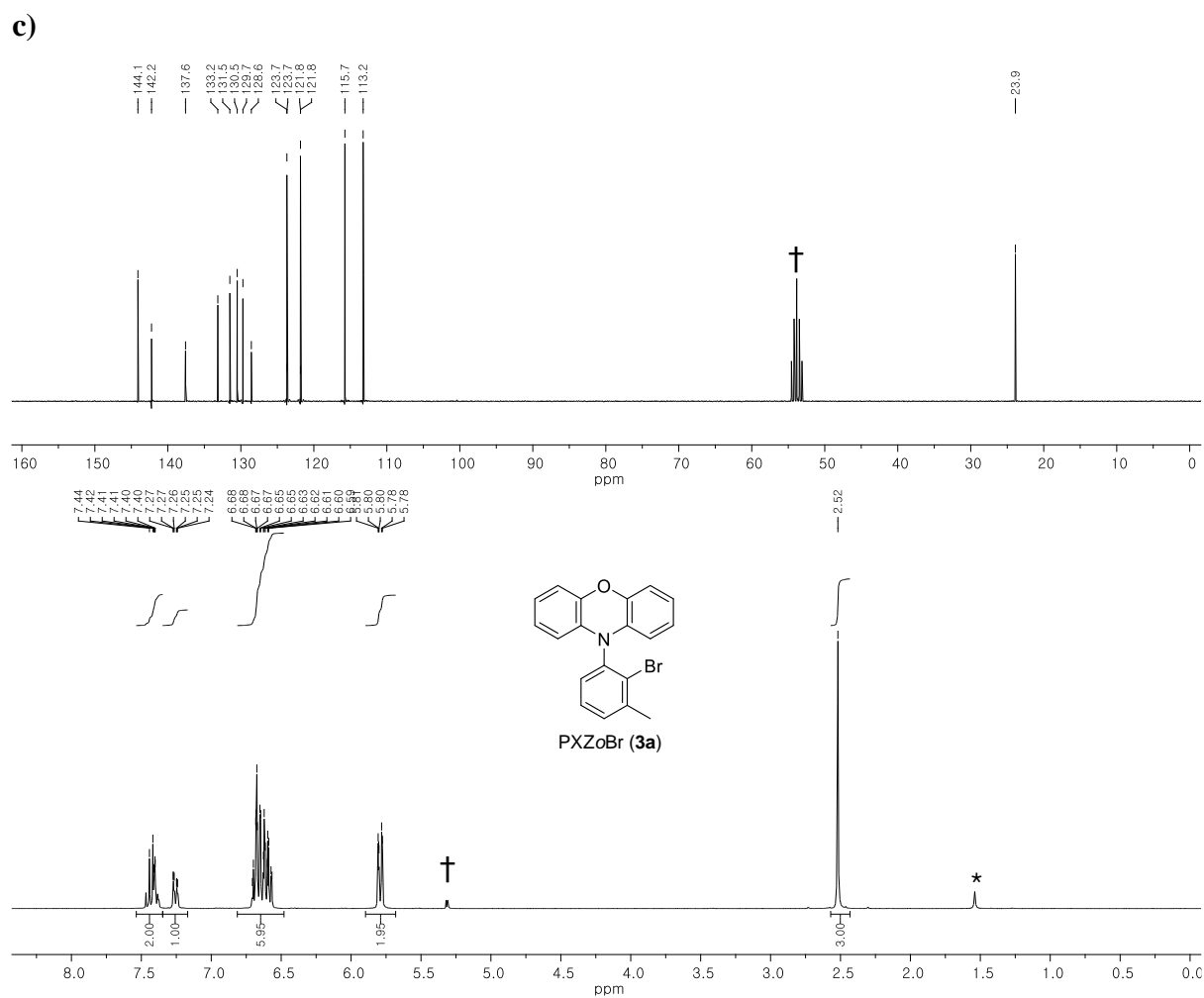
Figure 8. ^1H NMR spectra of **BuCzoBr** (a) in CDCl$_3$, ^1H (bottom) and ^{13}C (top) NMR spectra of **DMACoBr** (b) and **PXZoBr** (c) in CD$_2$Cl$_2$ (* from residual H$_2$O, † from CH$_2$Cl$_2$).
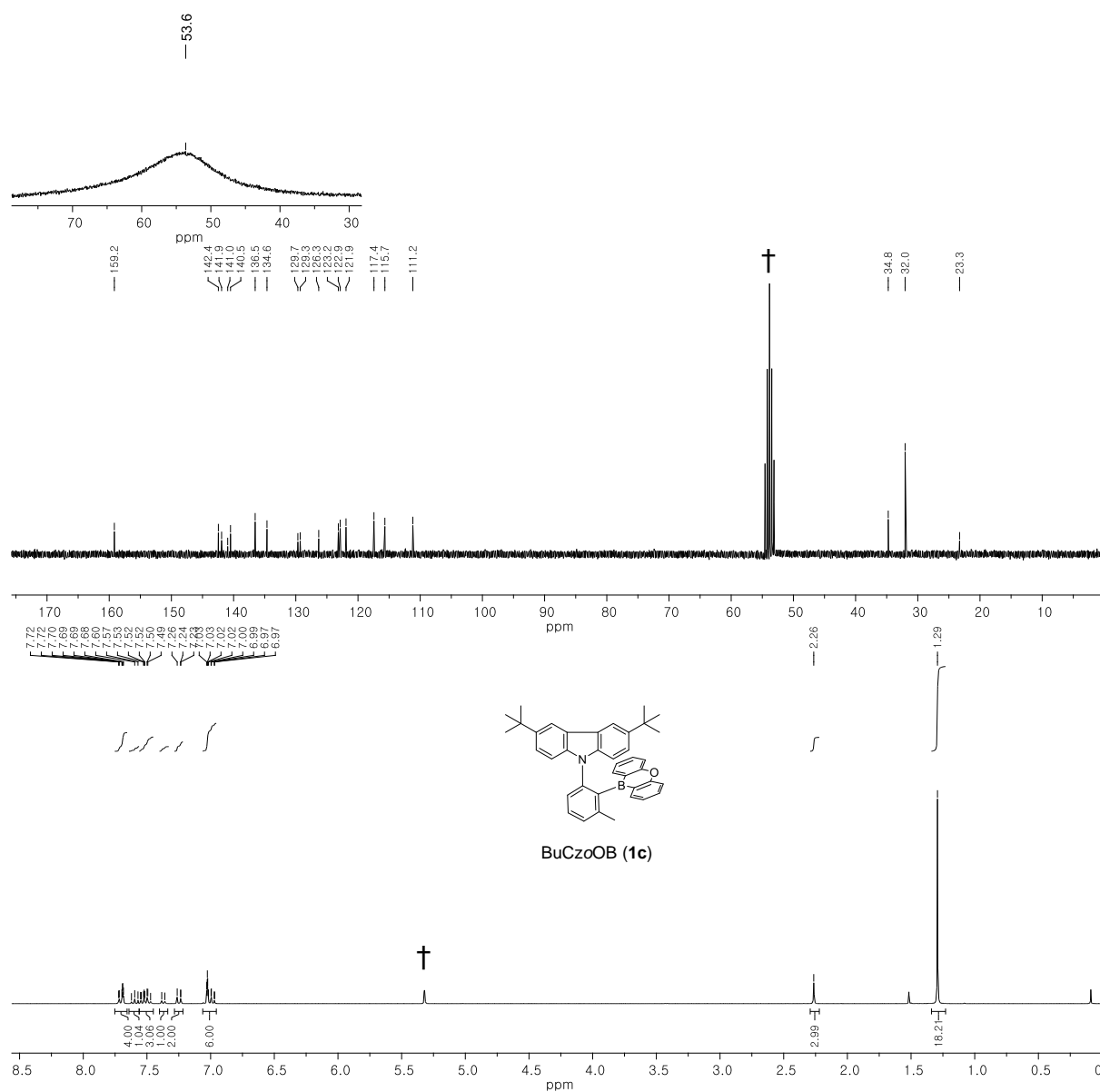
Figure 9. ^{1}H (bottom), ^{13}C (middle), and ^{11}B (top) NMR spectra of **BuCzoOB** in CD$_2$Cl$_2$ († from CH$_2$Cl$_2$).
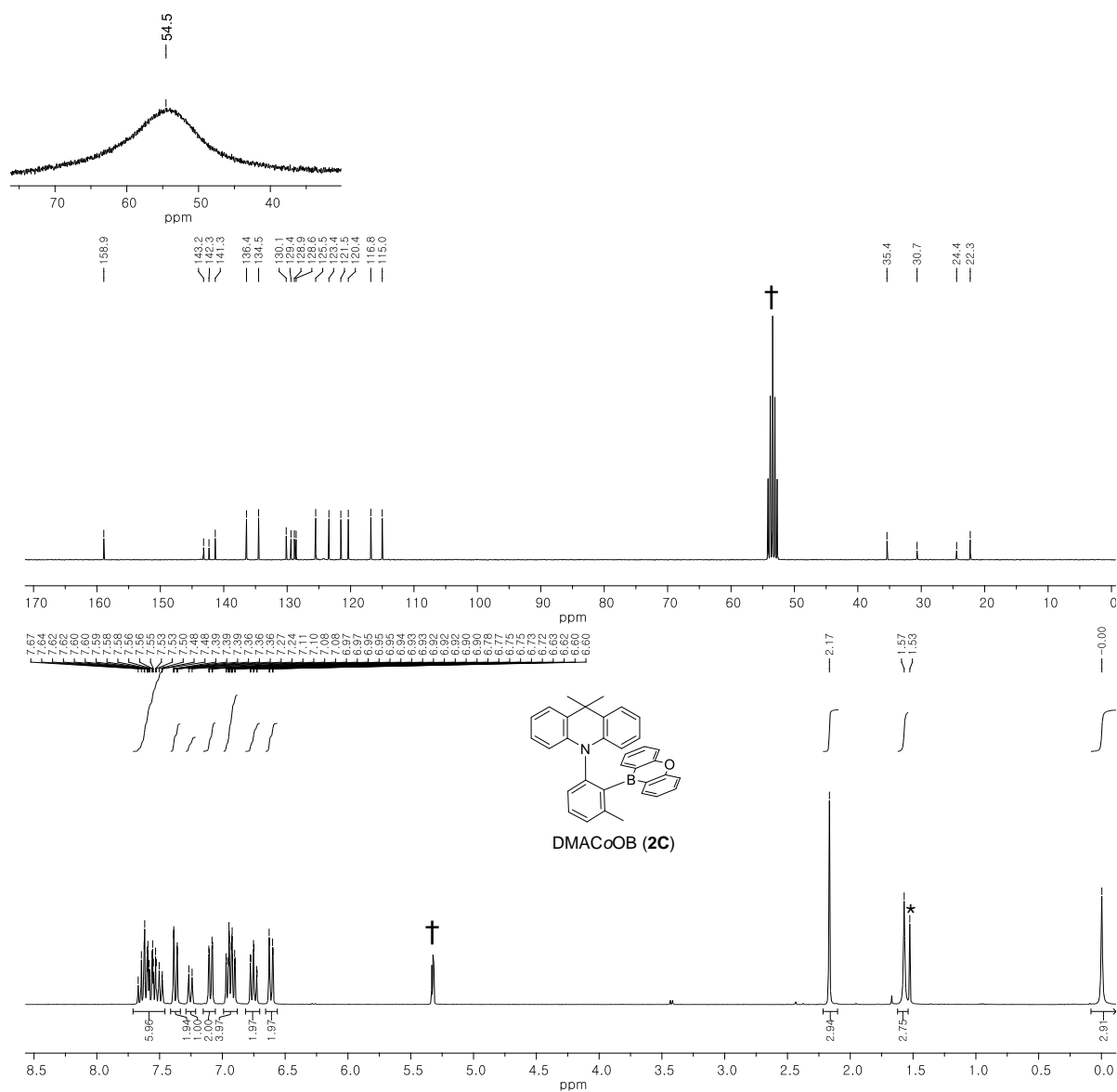
Figure 10. ^{1}H (bottom), ^{13}C (middle), and ^{11}B (top) NMR spectra of **DMACoOB** in CD$_2$Cl$_2$ (* from residual H$_2$O, † from CH$_2$Cl$_2$).
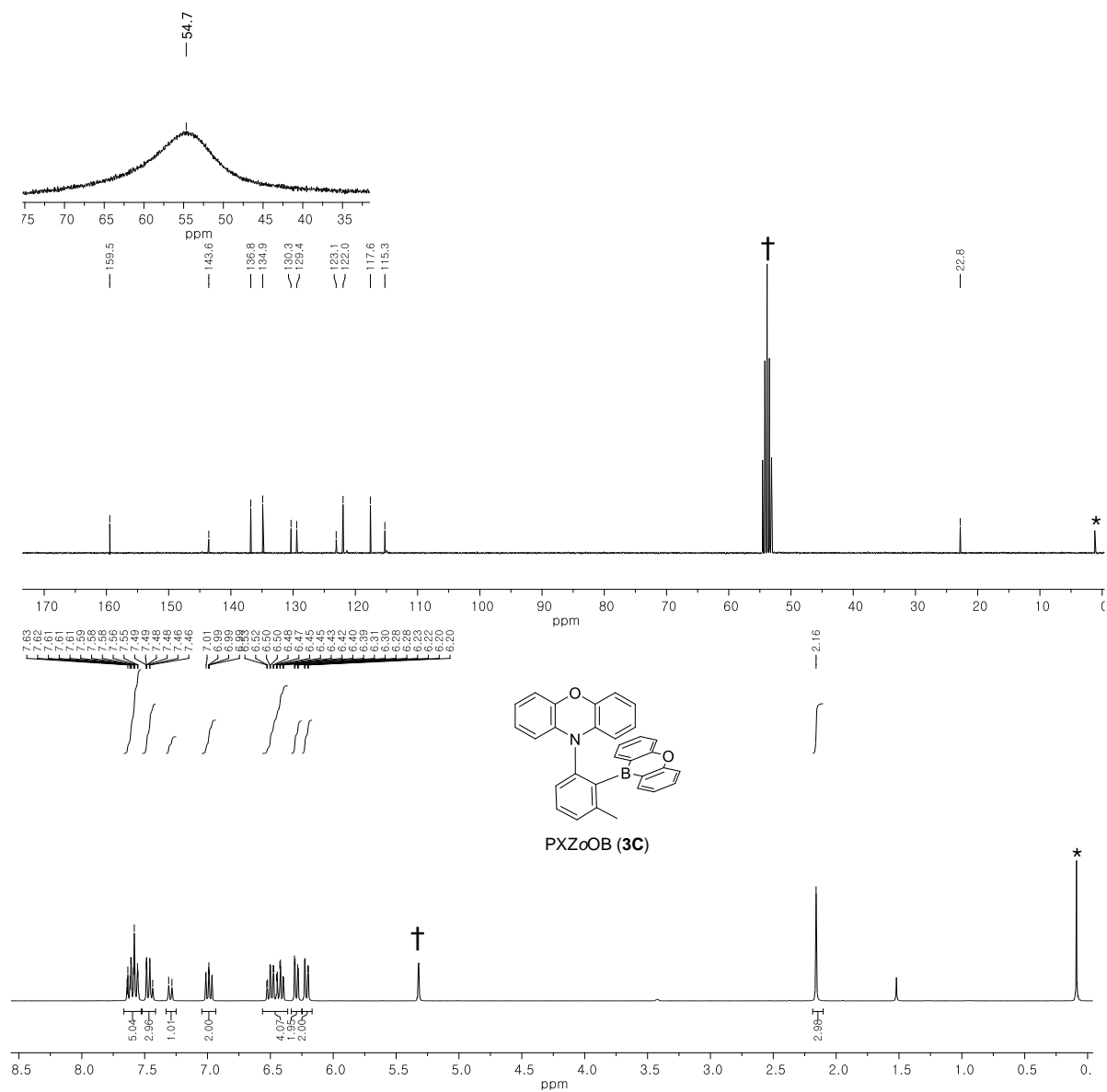
Figure 11. [1]H (bottom), ^{13}C (middle) and ^{11}B (top) NMR spectra of **PXZ*o*OB** in CD$_2$Cl$_2$ (*
from silicone grease, † from CH$_2$Cl$_2$).
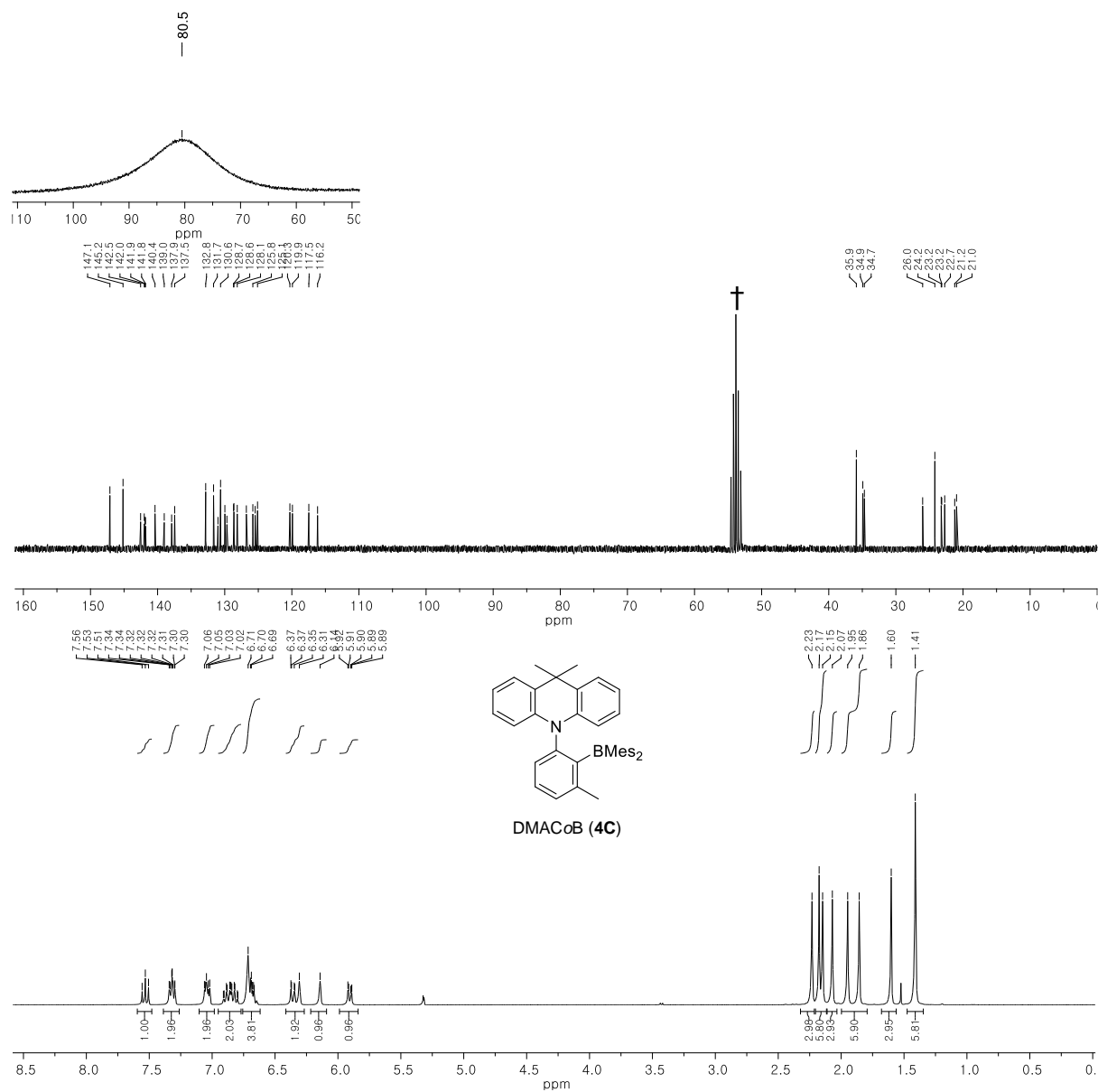
Figure 12. ^{1}H (bottom), ^{13}C (middle) and ^{11}B (top) NMR spectra of **DMAC*o*B** in CD$_2$Cl$_2$ († from CH$_2$Cl$_2$).

2. Crystal structure of DMAC*o*OB (2c) and DMAC*o*B (4c).

X-ray diffraction studies on **DMAC*o*OB** and **DMAC*o*B** distinctly showed the sterically congested nature in the *ortho* D−A compounds. To avoid congestion, the DMAC and oxaborin rings are perpendicular to the central phenyl ring, as judged by the dihedral angles of 90.0° respectively (**DMAC*o*OB**). A relative short distance between N(1) and B(1) of 2.845 Å was also observed confirming a direct N-B interaction for this series of compounds compared to **DAMC*o*B**. The detailed crystallographic data and the selected bond lengths and angles are given in Table. X-ray crystal structures are shown in (**Figure 13**).

Table 1. Selected bond lengths (Å) and angles (°) of **DMAC*o*OB** and **DMAC*o*B**

	DMAC*o*OB
Lengths(Å)	
B(1)–C(15)	1.581(3)
B(1)–C(17)	1.5319(19)
N(1)–C(1)	1.4155(15)
N(1)–C(10)	1.454(2)
C(10)–C(15)	1.382(3)
N(1)–B(1)	2.845
Angles (°)	
N(1)–C(10)–C(15)	118.15(17)
C(10)–C(15)–B(1)	119.38(17)
C(15)–B(1)–C(17)	122.56(9)

	DMAC*o*B
Lengths(Å)	
B(1)–C(21)	1.594(2)
B(1)–C(29)	1.575(2)
B(1)–C(23)	1.581(2)

N(1)–C(6)	1.4204(19)
N(1)–C(16)	1.4584(18)
C(16)–C(21)	1.407(2)
N(1)–B(1)	3.050
Angles (°)	
N(1)–C(16)–C(21)	121.24(13)
C(16)–C(21)–B(1)	123.49(12)
C(21)–B(1)–C(23)	119.98(13)
C(21)–B(1)–C(29)	119.38(13)
C(29)–B(1)–C(23)	120.57 (13)

Table 2. Crystallographic data and parameters for **DMAC*o*OB** and **DMAC*o*B**.

	DMAC*o*OB	DMAC*o*B
formula	$C_{34}H_{28}BNO$	$C_{40}H_{42}BN$
formula weight	477.43	547.61
crystal system	orthorhombic	triclinic
space group	*P*nma	*P*–1
a (Å)	10.21520(10)	8.1041(2)
b (Å)	14.4799(2)	12.5362(3)
c (Å)	19.4378(4)	15.6875(3)
α (°)	90	88.4884(11)
β (°)	90	88.1002(10)
γ (°)	90	74.4603(10)
V (Å^3)	2584.80(5)	1534.41(6)
Z	4	2
ρ_{calc} (g cm^{-3})	1.2267	1.1851
μ (mm^{-1})	0.072	0.067
$F(000)$	1008.4059	588.2117
T (K)	100	100
hkl range	$-12 \rightarrow 11, -17 \rightarrow 17,$ $-21 \rightarrow 21$	$-9 \rightarrow 7, -15 \rightarrow 14,$ $-18 \rightarrow 18$
measd reflns	33357	20436
unique reflns [R_{int}]	2468(0.0279)	5554(0.0221)
reflns used for refinement	2468	5554
refined parameters	208	388
R1[a] (I > 2σ(I))	0.0415	0.0437
wR2[b] all data	0.1033	0.1050
GOF on F^2	1.0860	1.0490
ρ_{fin} (max/min) (e Å^{-3})	0.1861/–0.2536	0.3058/–0.3696

[a] R1 = $\Sigma||Fo| - |Fc||/\Sigma|Fo|$. [b] wR2 = $\{[\Sigma w(Fo^2 - Fc^2)^2]/[\Sigma w(Fo^2)^2]\}^{1/2}$.

a)
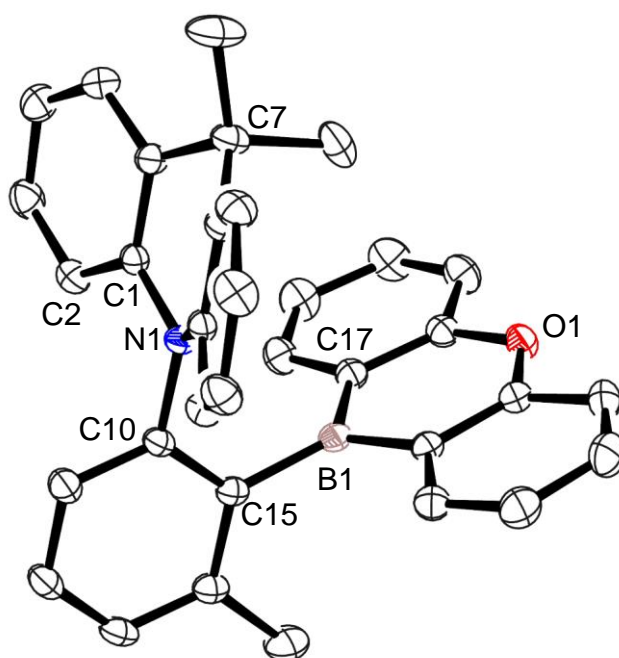
b)
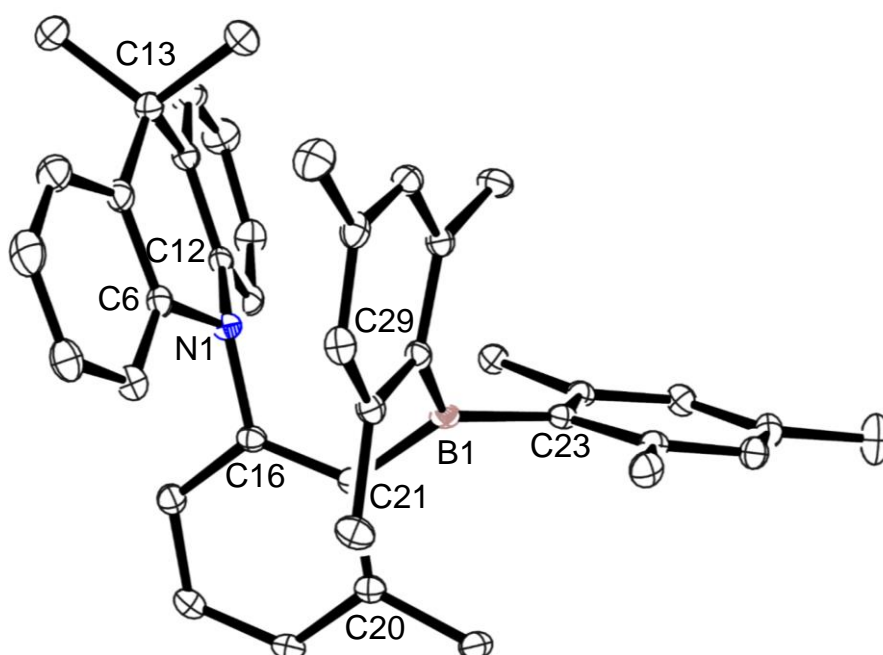
Figure 13. X-ray crystal structures of **DMAC*o*OB** and **DMAC*o*B** (30% thermal ellipsoids) with atom label. H atoms are omitted for clarity. Color code: blue = nitrogen; brown = boron; red = oxygen.

3. Photophysical Properties

The photophysical properties of all compounds, including UV/Vis absorption and photoluminescence (PL) spectra, were measured in degassed toluene (5.0×10^{-5} M) at 298 K. (**Figure 14** and **Table 3**). All the prepared compounds displayed strong absorption in the high energy region of 250−350 nm that absorption bands from DMAC, BuCz, PXZ-centered $\pi-\pi^*$ transition and the triarylboron-centered $\pi-p_\pi$(B) charge transfer (CT) transition.[4, 14] The broad low-energy absorptions (ca. 370−450 nm) can be resulted from intramolecular charge transfer (ICT) transition between the donor and triarylboron acceptors.[28] The PL spectra show different emission color ranging from blue to orange depending on the donor group (**BuCz*o*OB** = 459 nm; **DMAC*o*OB** = 488 nm; **PXZ*o*OB** = 540 nm).[19, 29] As for PLQY, compounds containing dimethylacridine donor exhibited high PLQY (**DMAC*o*OB** = 1.00; **DMAC*o*B** = 0.98) in oxygen free toluene. All compounds have the large decrease of the PLQY in air-saturated toluene that indicates quenching of the T_1 state by triplet oxygen, which in turn implies an efficient $T_1 \rightarrow S_1$ reverse intersystem crossing (RISC) in oxygen-free toluene (**Table 3**).[8, 9, 30] The transient PL decay curves of **2c**, **3c** and **4c** showed two decay components, i.e., the nanosecond-range prompt (τ_p) and microsecond-range delyed (τ_d) components at 298 K (**Figure 15**).[13, 20] A gradual increase in the emission intensity of the delayed component with increasing temperature from 120 to 290 K confirms that the observed delayed emission can be assigned to TADF (**Figure 16**).[13, 15, 21] The ΔE_{ST} values were determined experimentally from the fluorescence and phosphorescence spectra and were found to be in the rage of 3.7−11 meV, which are small to explain the strong TADF. (**Figure 17**, **Table 4**).[31, 32]

Table 3. Photophysical data of **BuCz*o*OB**, **DMAC*o*OB**, **PXZ*o*OB** and **DMAC*o*B**

Compound	$\lambda_{abs}{}^{a}$ [nm]	λ_{PL} [nm]		Φ_{PL} (%)		τ_p [ns (%)]^{c}	τ_d [μs (%)]^{d}	
		Toluene^{a}	PMMA	Toluene^{b} (N$_2$/air)	PMMA	Toluene	Toluene	PMMA
BuCz*o*OB	291, 345	459	448	66/10	77	175 (97)	$-^{e}$	14.8
DMAC*o*OB	288, 344, 376	488	481	100/7	100	66.0 (1)	8.33 (55)	10.8
PXZ*o*OB	333, 385	540	515	48/3	76	250 (2)	10.0 (75)	26.1
DMAC*o*B	298	531	518	98/5	100	135 (2)	5.74 (75)	8.5

$^{a)}$ In oxygen-free toluene at 298 K (5.0×10^{-5} M); $^{b)}$ Absolute photoluminescence quantum yields (PLQYs) in oxygen-free (N$_2$) and air-saturated (air) toluene at 298 K; $^{c)}$ PL lifetimes of prompt (τ_p) decay components for the air-saturated toluene solutions at 298 K. The estimated prompt (Φ_{PF}) portions (%) in transient decay curves are given in parentheses. $^{d)}$ PL lifetimes of delayed (τ_d) decay components (oxygen-free toluene solutions and film at 298 K). The estimated delayed (Φ_{DF}) portions (%) in transient decay curves are given in parentheses.; $^{e)}$ Not observed.
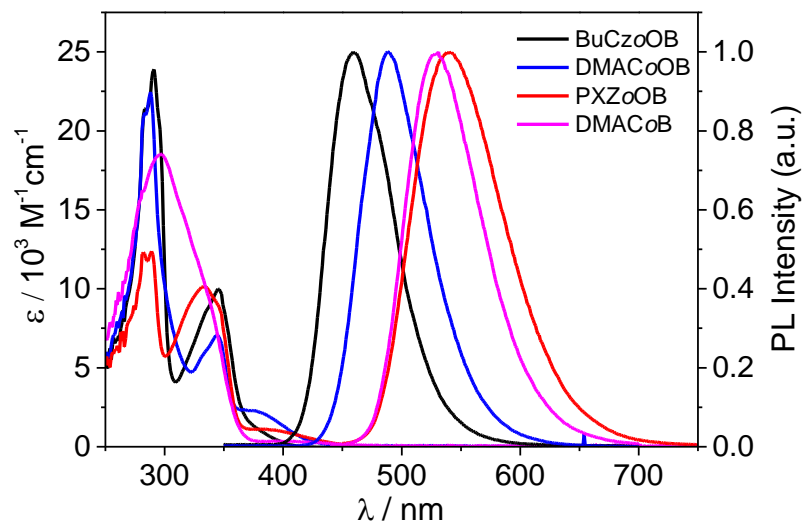
Figure 14. UV/vis absorption (left) and PL spectra (right) of **BuCz*o*OB**, **DMAC*o*OB**, **PXZ*o*OB and DMAC*o*B** in toluene (5.0×10^{-5} M) at 298 K.
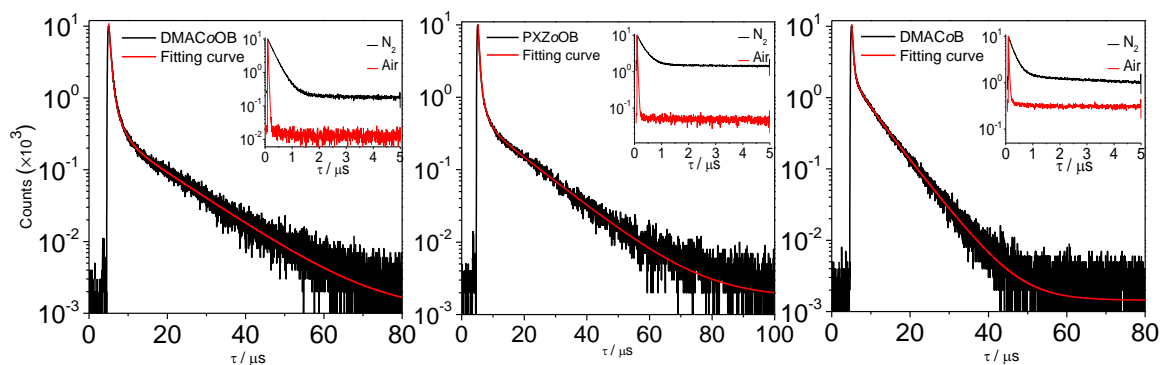
Figure 15. Transient PL decay curves of **DMAC*o*OB** (left), **PXZ*o*OB** (middle), **DMAC*o*B** (right) in oxygen-free toluene at 298 K. The inset shows the decay curves in oxygen-free (N_2) and air-saturated toluene.
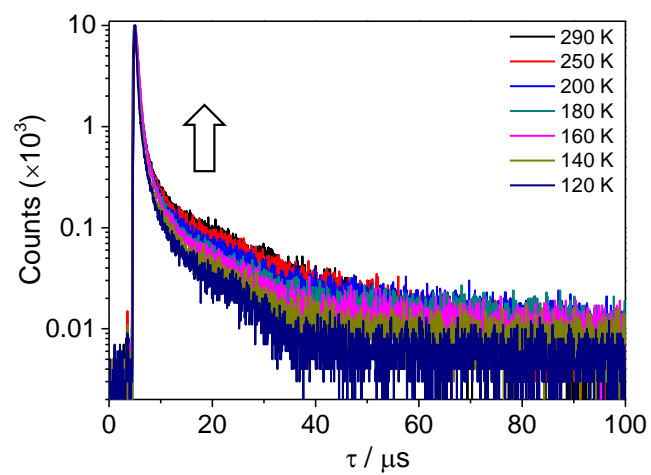
Figure 16. The temperature dependence of the transient PL decay curves from 120 to 290 K (**DMAC*o*OB**).
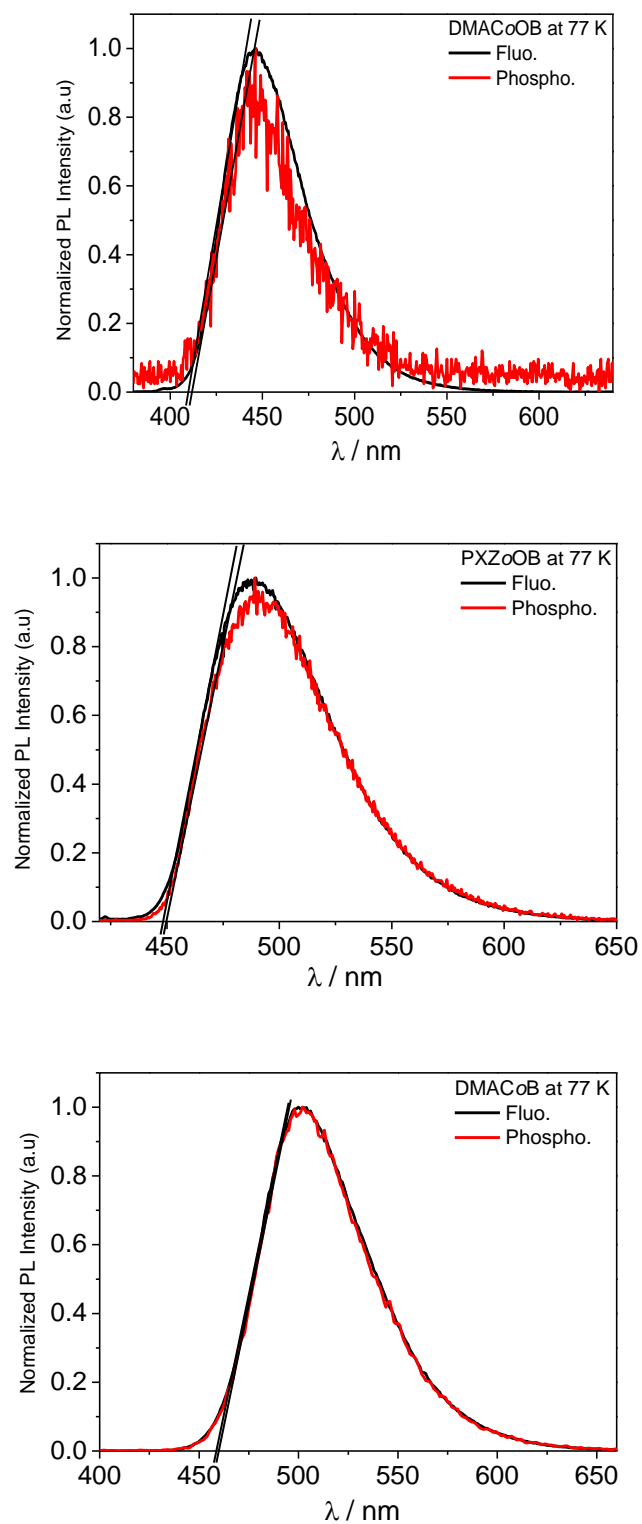
Figure 17. Fluorescence and phosphorescence spectra of **DMAC*o*OB** (top), **PXZ*o*OB** (middle) and **DMAC*o*B** (bottom) in toluene at 77 K.

Table 4. Photophysical data of **DMAC*o*OB**, **PXZ*o*OB** and **DMAC*o*B** at 77 K.

Compound	λ_{PL} [nm]	$E_S/E_T{}^a$ [eV]	$\Delta E_{ST}{}^b$ [meV]
DMAC*o*OB	446	3.038/3.034	3.7
PXZ*o*OB	489	2.784/2.773	11
DMAC*o*B	500	2.722/2.716	5.4

[a] E_S and E_T were calculated from the onset of fluorescence and phosphorescence spectra respectively. [b] $\Delta E_{ST} = E_S - E_T$.
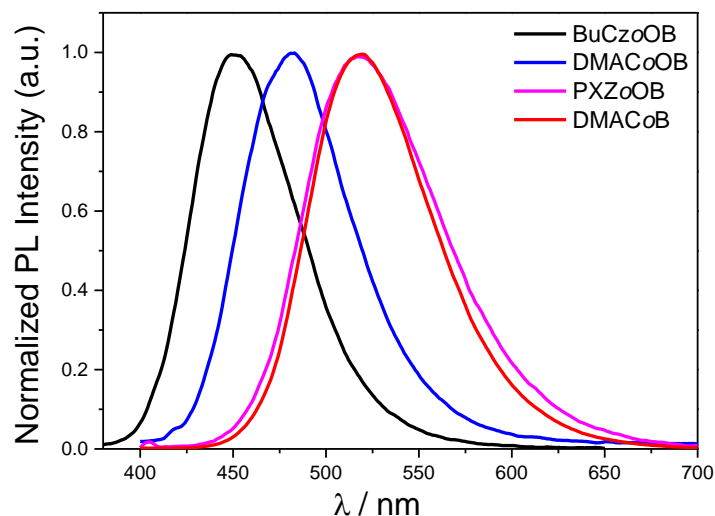
Figure 18. PL spectra of **BuCz*o*OB**, **DMAC*o*OB**, **PXZ*o*OB** and **DMAC*o*B** in PMMA film (10 wt%).

Photophysical properties were also measured in spin-coated PMMA film doped with 10% weight (10 wt%) of compounds (**Figure 18**). As the photophysical properties of all compounds doped within host films exhibit strong TADF with enhanced PLQYs compared to Toluene solution. In particular, **BuCz*o*OB** displayed delayed fluorescence (τ_d = 14.8 μs) compared to Toluene solution which not be observed delayed transient PL decay curve. All compounds were blue-shifted of ca. 7-25 nm compared to solution data (i.e. **BuCz*o*OB** = 459 nm; **DMAC*o*OB** = 488 nm; **PXZ*o*OB** = 540 nm; **DMAC*o*B** = 531 nm). All compounds in film also exhibit high PLQY in a value of 0.76-1.00.

4. Electrochemical Properties

The electrochemistry properties of **BuCzoOB**, **DMACoOB, PXZoOB** and **DMACoB** were carried out by cyclic voltammetry to understand the character of the frontier orbitals (**Figure 19** and **Table 5**). The half-wave oxidation potentials (E_{ox} versus Fc/Fc$^+$) were 0.72 V (**BuCzoOB**), 0.48 V (**DMACoOB**), 0.30 V (**PXZoOB**) and 0.42 (**DMACoB**) correspond to the reversible oxidation from donor moieties. **DMACoOB** and **DMACoB** showed similar oxidation potential due to the same moieties of dimethylacridine.[16] Consequently, their HOMO energy levels determined from the half-wave oxidation potentials were −5.52 eV, −5.28 eV, −5.10 eV and −5.22 eV respectively. The potentials positively shifted indicate that HOMO energy levels are gradually unstable as changed from *tert*-butyl carbazole to phenoxazine. As for reduction, all compounds showed reversible reduction potential due to the moieties of triarylboron compounds.[17, 31] The planarized triarylboron acceptor (**DMACoOB,** −2.42 eV) tend to have negatively shifting potential compared to non-planarized BMes$_2$ (**DMACoB**, −2.39 eV), giving more positive LUMO level. All reduction potentials estimated from the half-wave reduction potential, giving their calculated LUMO energy levels were −2.50 eV (**BuCzoOB**), −2.42 eV (**DMACoOB**), −2.48 eV (**PXZoOB**) and −2.39 eV (**DMACoB**) respectively.
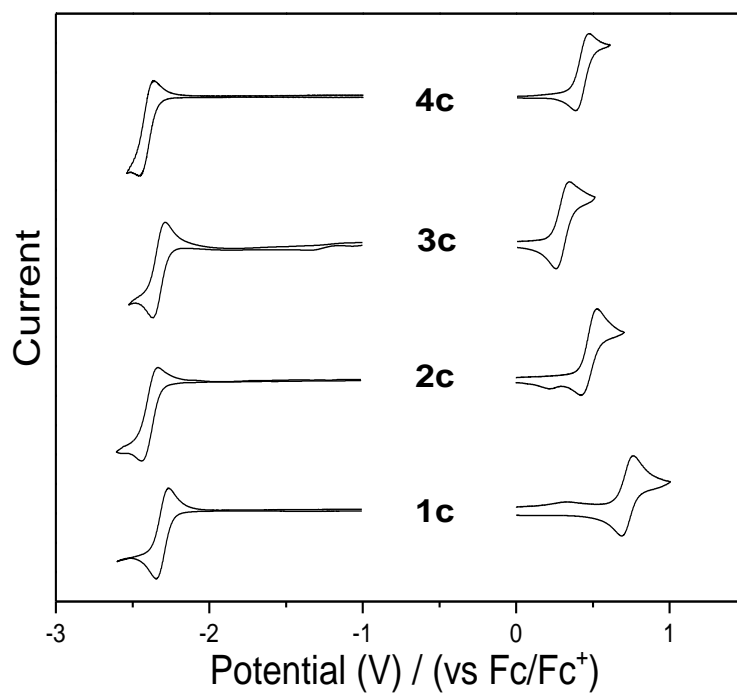
Figure 19. Cyclic voltammograms of **1c**–**4c** (1.0×10^{-3} M in MeCN, scan rate = 100 mV/s).

Table 5. Cyclic Voltammetry Data of **DMAC*o*OB**, **PXZ*o*OB**, and **DMAC*o*B**.

Compound	E_{ox} [V]	E_{red} [V]	HOMO/LUMO [eV]	$E_g{}^a$ [eV]
1c	0.72	−2.30	−5.52/−2.50	3.02
2c	0.48	−2.38	−5.28/−2.42	2.86
3c	0.30	−2.32	−5.10/−2.48	2.62
4c	0.42	−2.41	−5.22/−2.39	2.83

All reversible oxidation and reduction measured with reference to a Fc/Fc⁺ redox couple at 298 K. $^a E_g$ = LUMO − HOMO.

IV. Conclusion

Ortho-donor-acceptor containing oxaborin compounds (**1c–3c**) were prepared and characterized through NMR spectroscophy, X-ray crystallography, elemental analysis. Three compounds (**2c – 4c**) displayed strong TADF which was characterized by UV/Vis, PL, PLQY and lifetime measurements. In case of **BuCz*o*OB** (**1c**) showed delayed fluorescence in 10% PMMA film state. The compounds containing dimethylacridine as a donor exhibited high PLQY in oxygen free toluene solution (Φ_{PL} (%) = 100% for **2c**; 98% for **4c**). Attaching different substituents to the donor moieties of phenyl backbone led to shifting HOMO energy levels to unstable (**1c → 3c**). The twisted D–A structure which allowed for small ΔE_{ST} resulted in efficient TADF. From the X-ray crystal structure, we found direct interaction between N–B in **DMAC*o*OB** compared to **DMAC*o*B.** Especially, the DMAC and oxaborin rings are perpendicular to the central phenyl ring, as judged by the dihedral angles of 90.0° respectively (**DMAC*o*OB**). The result from this study gives the prospect as a third generation OLED emitting material containing the newly introduced oxaborin electron acceptor.

V. Reference

1.　Tang, C. W.; VanSlyke, S. A., Organic electroluminescent diodes. *Appl. Phys. Lett.* **1987,** *51* (12), 913-915.

2.　Helfrich, W.; Schneider, W. G., Recombination Radiation in Anthracene Crystals. *Phys. Rev. Lett.* **1965,** *14* (7), 229-231.

3.　Tao, Y.; Yang, C.; Qin, J., Organic host materials for phosphorescent organic light-emitting diodes. *Chem. Soc. Rev.* **2011,** *40* (5), 2943-70.

4.　Chen, X. L.;　Jia, J. H.;　Yu, R.;　Liao, J. Z.;　Yang, M. X.; Lu, C. Z., Combining Charge-Transfer Pathways to Achieve Unique Thermally Activated Delayed Fluorescence Emitters for High-Performance Solution-Processed, Non-doped Blue OLEDs. *Angew. Chem.., Int. Ed.***2017,** *56* (47), 15006-15009.

5.　Fan, C.; Yang, C., Yellow/orange emissive heavy-metal complexes as phosphors in monochromatic and white organic light-emitting devices. *Chem. Soc. Rev.* **2014,** *43* (17), 6439-69.

6.　Kappaun, S.;　Slugovc, C.; List, E. J., Phosphorescent organic light-emitting devices: working principle and iridium based emitter materials. *Int. J. Mol. Sci.* **2008,** *9* (8), 1527-47.

7.　Jou, J.-H.;　Kumar, S.;　Agrawal, A.;　Li, T.-H.; Sahoo, S., Approaches for fabricating high efficiency organic light emitting diodes. *J.Mater. Chem. C* **2015,** *3* (13), 2974-3002.

8.　Lin, T. A.;　Chatterjee, T.;　Tsai, W. L.;　Lee, W. K.;　Wu, M. J.;　Jiao, M.;　Pan, K. C.;　Yi, C. L.;　Chung, C. L.;　Wong, K. T.; Wu, C. C., Sky-Blue Organic Light Emitting Diode with 37% External Quantum Efficiency Using Thermally Activated Delayed Fluorescence from Spiroacridine-Triazine Hybrid. *Adv. Mater.* **2016,** *28* (32), 6976-83.

9.　Kitamoto, Y.;　Namikawa, T.;　Ikemizu, D.;　Miyata, Y.;　Suzuki, T.;　Kita, H.; Sato, T.; Oi, S., Light blue and green thermally activated delayed fluorescence from 10H-phenoxaborin-derivatives and their application to organic light-emitting diodes. *J.Mater. Chem. C* **2015,** *3* (35), 9122-9130.

10.　Chi, Y.; Chou, P. T., Transition-metal phosphors with cyclometalating ligands: fundamentals and applications. *Chem. Soc. Rev.* **2010,** *39* (2), 638-55.

11.　Godumala, M.;　Choi, S.;　Cho, M. J.; Choi, D. H., Thermally activated delayed fluorescence blue dopants and hosts: from the design strategy to organic light-emitting diode

applications. *J.Mater. Chem. C* **2016,** *4* (48), 11355-11381.

12.　Manna, M. K.;　Shokri, S.;　Wiederrecht, G. P.;　Gosztola, D. J.; Ayitou, A. J., New perspectives for triplet-triplet annihilation based photon upconversion using all-organic energy donor & acceptor chromophores. *Chem. Commun.* **2018,** *54* (46), 5809-5818.

13.　Lee, S. Y.;　Adachi, C.; Yasuda, T., High-Efficiency Blue Organic Light-Emitting Diodes Based on Thermally Activated Delayed Fluorescence from Phenoxaphosphine and Phenoxathiin Derivatives. *Adv. Mater.* **2016,** *28* (23), 4626-31.

14.　Uoyama, H.;　Goushi, K.;　Shizu, K.;　Nomura, H.; Adachi, C., Highly efficient organic light-emitting diodes from delayed fluorescence. *Nature* **2012,** *492* (7428), 234-8.

15.　Liu, Y.;　Li, C.;　Ren, Z.;　Yan, S.; Bryce, M. R., All-organic thermally activated delayed fluorescence materials for organic light-emitting diodes. *Nat. Rev. Mater.* **2018,** *3* (4).

16.　Kitamoto, Y.;　Namikawa, T.;　Suzuki, T.;　Miyata, Y.;　Kita, H.;　Sato, T.; Oi, S., Dimesitylarylborane-based luminescent emitters exhibiting highly-efficient thermally activated delayed fluorescence for organic light-emitting diodes. *Org. Electron.* **2016,** *34*, 208-217.

17.　Numata, M.;　Yasuda, T.; Adachi, C., High efficiency pure blue thermally activated delayed fluorescence molecules having 10H-phenoxaborin and acridan units. *Chem. Commun.* **2015,** *51* (46), 9443-6.

18.　Zhang, Q.;　Tsang, D.;　Kuwabara, H.;　Hatae, Y.;　Li, B.;　Takahashi, T.;　Lee, S. Y.;　Yasuda, T.;　Adachi, C., Nearly 100% internal quantum efficiency in undoped electroluminescent devices employing pure organic emitters. *Adv. Mater.* **2015,** *27* (12), 2096-100.

19.　Kumar, A.;　Oh, J.;　Kim, J.;　Jung, J.;　Lee, M. H., Facile color tuning of thermally activated delayed fluorescence by substituted ortho-carbazole-appended triarylboron emitters. *Dyes and Pigments.* **2019,** *168*, 273-280.

20.　Lee, Y. H.;　Park, S.;　Oh, J.;　Woo, S.-J.;　Kumar, A.;　Kim, J.-J.;　Jung, J.; Yoo, S.; Lee, M. H., High-Efficiency Sky Blue to Ultradeep Blue Thermally Activated Delayed Fluorescent Diodes Based on Ortho-Carbazole-Appended Triarylboron Emitters: Above 32% External Quantum Efficiency in Blue Devices. *Adv. Opt. Mater.* **2018,** *6* (17).

21. Lee, Y. H.; Park, S.; Oh, J.; Shin, J. W.; Jung, J.; Yoo, S.; Lee, M. H., Rigidity-Induced Delayed Fluorescence by Ortho Donor-Appended Triarylboron Compounds: Record-High Efficiency in Pure Blue Fluorescent Organic Light-Emitting Diodes. *ACS Appl. Mater. Interfaces* **2017,** *9* (28), 24035-24042.

22. Wong, M. Y.; Zysman-Colman, E., Purely Organic Thermally Activated Delayed Fluorescence Materials for Organic Light-Emitting Diodes. *Adv. Mater.* **2017,** *29* (22).

23. HUDSON, Z. M.; WANG, S., <Wang BN-AccChemRes-2009.pdf>. **2009**.

24. Huang, T.; Jiang, W.; Duan, L., Recent progress in solution processable TADF materials for organic light-emitting diodes. *J. Mater. Chem. C* **2018,** *6* (21), 5577-5596.

25. Ikeuchi, T.; Inuki, S.; Oishi, S.; Ohno, H., Gold(I)-Catalyzed Cascade Cyclization Reactions of Allenynes for the Synthesis of Fused Cyclopropanes and Acenaphthenes. *Angew. Chem., Int Ed* **2019,** *58* (23), 7792-7796.

26. Gilman, H.; Miles, D., Some Organosilicon Compounds Derived from Phenyl Ether. *J. Org. Chem.* **1958,** *23* (9), 1363-1365.

27. Melaımi, M.; Sole, S. p.; Chiu, C.-W.; Wang, H.; Gabbaı, F. P., <Gabbai-oxaboraanthracene-IC-2006.pdf>. **2006**.

28. Meng, G.; Chen, X.; Wang, X.; Wang, N.; Peng, T.; Wang, S., Isomeric Bright Sky-Blue TADF Emitters Based on Bisacridine Decorated DBNA: Impact of Donor Locations on Luminescent and Electroluminescent Properties. *Adv. Opt. Mater.* **2019,** *7* (11).

29. Kim, J. H.; Yun, J. H.; Lee, J. Y., Recent Progress of Highly Efficient Red and Near-Infrared Thermally Activated Delayed Fluorescent Emitters. *Adv. Opt. Mater.* **2018,** *6* (18).

30. Zhang, Q.; Li, J.; Shizu, K.; Huang, S.; Hirata, S.; Miyazaki, H.; Adachi, C., Design of efficient thermally activated delayed fluorescence materials for pure blue organic light emitting diodes. *J. Am. Chem. Soc.* **2012,** *134* (36), 14706-9.

31. Suzuki, K.; Kubo, S.; Shizu, K.; Fukushima, T.; Wakamiya, A.; Murata, Y.; Adachi, C.; Kaji, H., Triarylboron-Based Fluorescent Organic Light-Emitting Diodes with External Quantum Efficiencies Exceeding 20. *Angew. Chem., Int Ed* **2015,** *54* (50), 15231-5.

32. Oita, K.; Gilman, H., The Preparation of Some Derivatives of Phenoxasilin, a Silicon Analog of Xanthene. *J. Am. Chem. Soc.* **1957,** *79* (2), 339-342.